Cell Reports
Medicine

Article

T cell-attracting CCL18 chemokine is a dominant rejection signal during limb transplantation

Graphical abstract

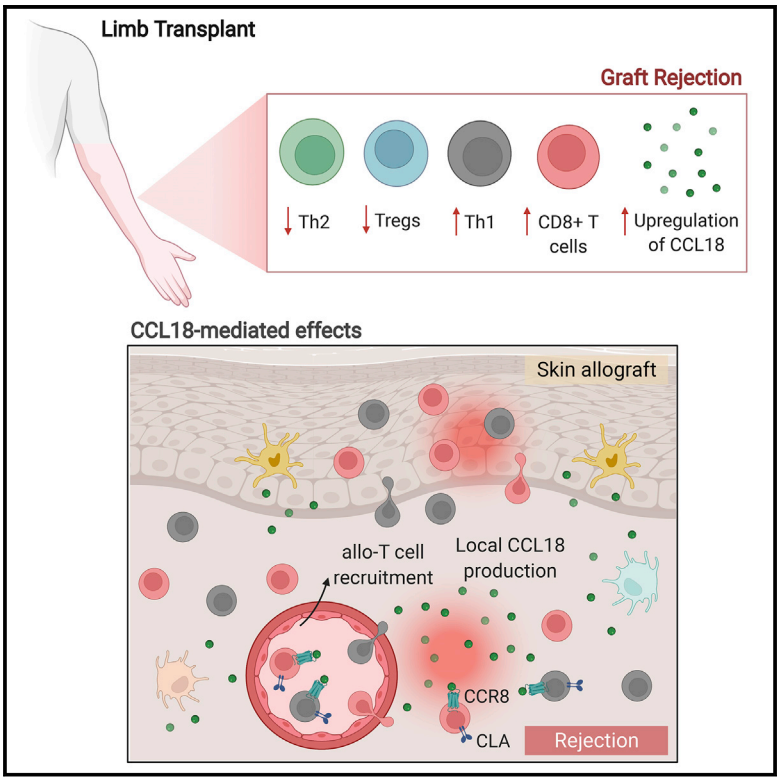

Highlights

- Increased T cell infiltration in the stable graft compared with native skin
- The chemokine CCL18 is upregulated during rejection in limb transplantation
- CCL18 recruits more allo-T cells to the skin and leads to accelerated xenograft loss
- CCR8 blockade halts CCL18-mediated T cell infiltration

Authors

Thiago J. Borges, Phammela Abarzua, Rodrigo B. Gassen, ..., Christine G. Lian, Simon G. Talbot, Leonardo V. Riella

Correspondence

lriella@mgh.harvard.edu

In brief

Borges et al. provide a comprehensive immune characterization of limb transplant recipients, demonstrating that the chemokine CCL18 is a dominant signal during rejection. Local CCL18 mediates recruitment of pathogenic allo-T cells into grafts, which is abrogated by CCR8 blockade. Targeting the CCL18:CCR8 pathway is a promising complementary immunosuppressive approach in transplantation.

Borges et al., 2022, Cell Reports Medicine *3*, 100559
March 15, 2022
https://doi.org/10.1016/j.xcrm.2022.100559

CellPress

Cell Reports Medicine

CellPress
OPEN ACCESS

Article

T cell-attracting CCL18 chemokine is a dominant rejection signal during limb transplantation

Thiago J. Borges,[1,2] Phammela Abarzua,[3] Rodrigo B. Gassen,[2] Branislav Kollar,[4,5] Mauricio Lima-Filho,[1] Bruno T. Aoyama,[1] Diana Gluhova,[6] Rachael A. Clark,[7] Sabina A. Islam,[8] Bohdan Pomahac,[4] George F. Murphy,[3] Christine G. Lian,[3] Simon G. Talbot,[4] and Leonardo V. Riella[1,2,9,10,*]

[1]Schuster Family Transplantation Research Center, Renal Division, Brigham and Women's Hospital, Harvard Medical School, Boston, MA 02115, USA

[2]Center for Transplantation Sciences, Department of Surgery, Massachusetts General Hospital, Harvard Medical School, Boston, MA 02129, USA

[3]Program in Dermatopathology, Department of Pathology, Brigham and Women's Hospital, Boston, MA 02115, USA

[4]Division of Plastic Surgery, Department of Surgery, Brigham and Women's Hospital, Harvard Medical School, Boston, MA 02115, USA

[5]Department of Plastic and Hand Surgery, University of Freiburg Medical Center, University of Freiburg Faculty of Medicine, 79106 Freiburg, Germany

[6]DF/HCC Specialized Histopathology Core – Massachusetts General Hospital Site, Boston, MA 02129, USA

[7]Department of Dermatology, Brigham and Women's Hospital, Harvard Medical School, Boston MA 02115, USA

[8]Center for Immunology and Inflammatory Diseases, Division of Rheumatology, Allergy and Immunology, Massachusetts General Hospital, Harvard Medical School, Boston, MA 02129, USA

[9]Division of Nephrology, Massachusetts General Hospital, Harvard Medical School, Boston, MA 02114, USA

[10]Lead contact

*Correspondence: lriella@mgh.harvard.edu

https://doi.org/10.1016/j.xcrm.2022.100559

SUMMARY

Limb transplantation is a life-changing procedure for amputees. However, limb recipients have a 6-fold greater rejection rate than solid organ transplant recipients, related in part to greater immunogenicity of the skin. Here, we report a detailed immunological and molecular characterization of individuals who underwent bilateral limb transplantation at our institution. Circulating Th17 cells are increased in limb transplant recipients over time. Molecular characterization of 770 genes in skin biopsies reveals upregulation of T cell effector immune molecules and chemokines, particularly CCL18. Skin antigen-presenting cells primarily express the chemokine CCL18, which binds to the CCR8 receptor. CCL18 treatment recruits more allo-T cells to the skin xenograft in a humanized skin transplantation model, leading to signs of accelerated graft rejection. Blockade of CCR8 remarkedly decreases CCL18-induced allo-T cell infiltration. Our results suggest that targeting the CCL18:CCR8 pathway could be a promising immunosuppressive approach in transplantation.

INTRODUCTION

Vascularized composite allotransplantation (VCA), including limb transplantation, is a life-changing procedure for individuals who have suffered severe traumatic injuries. Unlike solid organ transplantation, VCA involves transplantation of multiple tissues with different immunogenicity levels, including skin, muscle, bones, and nerves. Among these, the skin has the highest immunogenicity of all[1] because of the presence of the following components: a dense population of antigen-presenting cells (APCs) and resident T cells, a rich microbiota, and continuous exposure to environmental threats, both physical and chemical. These unique skin features may explain the 6-fold greater rejection rate of VCA recipients compared with solid organ transplant recipients.[2] More than 85% of individuals undergoing VCA experience acute cellular rejection in the first year after transplantation, and many have multiple episodes of rejection, leading to a higher burden of immunosuppressive therapy over time.[3] It is reported that the number of rejection episodes may portend forthcoming chronic rejection events and graft loss.[2] A better understanding of key distinctions between VCA and solid organ transplantation immune responses is essential for discovery of novel markers of rejection and predictive biomarkers.

Here we identified unique molecular signatures in skin graft biopsies at times of rejection that were dominated by T-effector molecules and chemokines, particularly CCL18. The CCL18 chemokine is present only in primates, with no murine ortholog, and has been identified as a key chemokine in the skin. CCL18 has been described to bind to the CCR8 receptor[4] and induce homing of T cells in inflammatory skin conditions.[5–7] Based on the unique rejection signal on graft biopsies, we sought to investigate the role of CCL18 in skin transplantation. By using a humanized skin transplantation model, we observed that CCL18 treatment recruited more allo-T cells to the skin and led to accelerated damage of the xenograft. This effect was abrogated markedly by treating the recipients with an anti-CCR8 blocking antibody. We

Table 1. Baseline characteristics of upper extremity transplant recipients and donors

	Individual 1	Individual 2	Individual 3
Recipient characteristics			
Age at transplantation (years)	65	40	30
Sex	male	male	male
Ethnicity	white	white	white
Cause of injury	septic shock	septic shock	ballistic trauma
Surgery	bilateral forearm	bilateral upper extremity	bilateral upper extremity
PRA (%)	0	69	0
Donor-specific antibodies	negative	positive	negative
HLA mismatch (A, B, DR)	5/6	5/6	4/6
CMV status	negative	negative	negative
EBV status	positive	positive	positive
Induction agent	thymoglobulin	thymoglobulin	thymoglobulin
Follow-up (years)	9	6	4
Donor characteristics			
Age (years)	44	23	27
Sex	male	male	male
CMV status	negative	negative	negative
EBV status	positive	positive	positive
Total ischemia time (hours)	4	4	4 right/5 left

characterized immunological changes in the graft microenvironment compared with proximal native skin tissue. Our data suggest an increase in T cell infiltration and action in the graft microenvironment compared with native tissue. We demonstrated a role of the chemokine CCL18 in attracting inflammatory allo-T cells to skin grafts, identifying the CCL18-CCR8 pathway as a potential therapeutic target in transplantation.

RESULTS

Expansion of circulating Th17 cells after transplantation

Th17 cells have a pathogenic role in different skin inflammatory disorders.[8,9] We reasoned that Th17 cells would be enriched over time upon limb transplantation. Three individuals who received limb transplants in our institution between October 2011 and August 2016 were included in this analysis, with a mean follow-up of 5.2 years. The clinical characteristics of these individuals are detailed in Table 1. The individuals' pre- and post-operative appearance is shown in Figure S1. Detailed information about the individuals' immunosuppression is given in the STAR methods. We initially characterized T cell subsets from peripheral blood collected over time after transplantation according to our protocol (pre-transplantation, 24 h, 1 week, and 3, 6, and 12 months; Figure 1A). Analyses of the effector and memory T cell subsets (Figure S2) revealed that $CD4^+$ central memory T cells (TCM cells; $CD45RA^-CCR7^+$) were the predominant T cell phenotype in the pool of $CD4^+$ T cells, although they decreased after transplantation, whereas $CD4^+$ effector memory T cells (TEMs; $CD45RA^-CCR7^-$) increased over time (Figure 1B). TEMs and effector memory $CD45RA^+$ T cells (TEMRA cells; $CD45RA^+CCR7^-$) were the main subsets presented in the pool of $CD8^+$ T cells with a decrease in naive $CD8^+$ T cells ($CD45RA^+CCR7^+$) after transplantation (Figure 1C). Next, we assessed the T helper (Th) phenotypes based on CXCR3 and CCR6 expression (Figure 1D). Circulating Th2 cells were the predominant phenotype in individuals with upper extremity transplantation over time (Figure 1E). Th17 cells were increased markedly after transplantation (Figure 1F), whereas Th1 cells were stable over time (Figure 1E). The percentage of circulating regulatory T (Treg) cells ($CD4^+CD25^+CD127^{-/low}$ cells; Figure 1G) and T follicular helper (Tfh) cells ($CD4^+CXCR5^+PD\text{-}1^+$ cells; Figure 1H) had no significant expansion after transplantation, other than transient changes early after transplantation, likely related to use of depletion induction therapy. These findings indicate that Th2 cells were the dominant phenotype over time after transplantation, with a significant expansion of circulating Th17 cells.

Increased T cell infiltration and activation in the non-rejecting graft microenvironment compared with native skin

In transplantation, characterization of the T cells infiltrating human allografts compared with native tissues is technically limited by the small sample sizes collected in punch biopsies. We took advantage of debulking surgeries performed in our limb transplant recipients to examine T cells in the graft microenvironment at nonrejection time points and compared it with recipients' adjacent native skin removed during the procedure. Allografts and native skins were processed, and infiltrating cells were isolated and stained by flow cytometry (Figure S3). Allografts had higher frequencies of activated $CD4^+$ T cells, including $CD4^+$ TEM cells (Figure 2A), Th1 cells ($CD4^+CXCR3^+CCR6^-$; Figure 2B), and Th17 cells ($CD4^+CXCR3^-CCR6^+$; Figure 2C) compared with native skin. Similarly, total $CD8^+$ cells (Figure 2D), $CD8^+$ TEM (Figure 2E) and TEMRA cells (Figure 2F) were also increased markedly compared with native skin. Immunofluorescence

CellPress
OPEN ACCESS

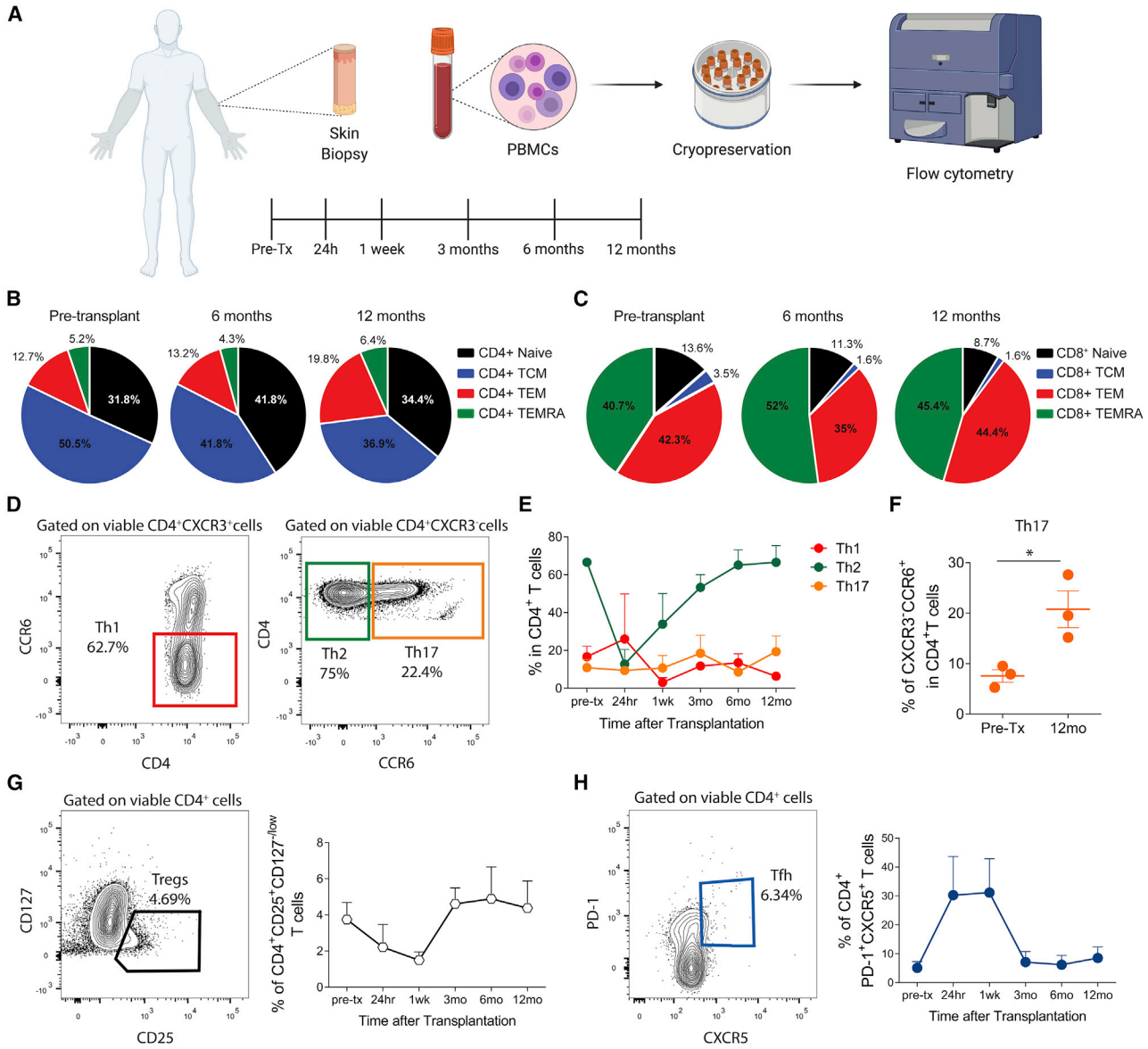

Figure 1. Analysis of circulating CD4⁺ and CD8⁺ T cell subsets from upper extremity recipients over time

(A) Skin biopsies and peripheral blood were collected over time (pre-transplantation, 24 h, 1 week, and 3, 6, and 12 months after transplantation) from upper extremity transplant recipients. PBMCs were isolated for posterior flow cytometry analysis. The cartoon was created with BioRender.

(B and C) Mean percentages of blood CD4⁺ (B) and CD8⁺ (C) naive cells (CCR7⁺CD45RA⁺), central memory T cells (TCM cells; CCR7⁺CD45RA⁻), effector memory T cells (TEM cells; CCR7⁻CD45RA⁻), and effector memory RA cells (TEMRA cells; CCR7⁻CD45RA⁺) before transplantation and 6 and 12 months after transplantation, represented as pie charts. Data are from all three individuals.

(D) Representative contour plots of gating of T helper (Th) 1 (CD4⁺CXCR3⁺CCR6⁻), Th2 (CD4⁺CXCR3⁻CCR6⁻), and Th17 (CD4⁺CXCR3⁻CCR6⁺) cells.

(E) Mean percentages of Th1, Th2, and Th17 cells from all three individuals over time.

(F–H) Mean percentages of circulating Th17 cells before transplantation and 12 months after transplantation. Statistic by paired t test, *$p < 0.05$. (G and H) Representative contour plots and mean percentages of (G) regulatory T (Treg) cells (CD4⁺CD25⁺CD127$^{-/low}$) and (H) T follicular helper (Tfh) cells (CD4⁺CXCR5⁺PD-1⁺) from all three individuals over time.

Graphs are displayed as mean ± SD at each time point examined.

See also Figures S1and S2.

analyses of skin biopsies confirmed an increased influx of CD4⁺ and CD8⁺ cells in the allograft tissue compared with recipients' adjacent native skin (Figure 2G), with approximately 5–10 positively labeled cells per vascular profile (CD8:CD4 ratio approximately 1:1) in allografts versus only rare ones (1–2 T cells per vascular profile) in adjacent native skin. Our data suggest that the graft microenvironment with alloantigens favors infiltration, expansion, and activation of T cells locally.

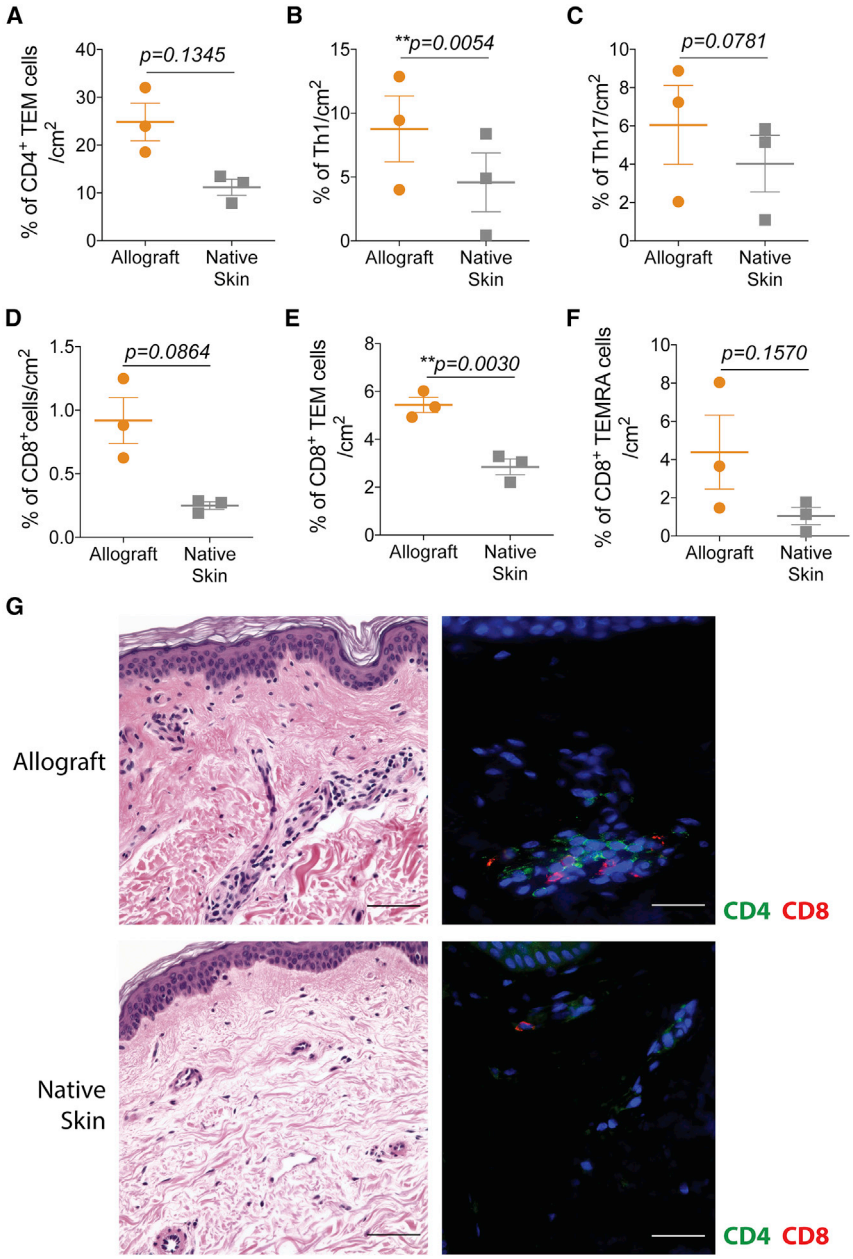

Figure 2. Characterization of CD4⁺ and CD8⁺ T cell subsets from allografts and native skin of upper extremity recipients

(A–F) Mean percentages per skin area of infiltrating (A) $CD4^+$ TEM cells ($CCR7^-CD45RA^-$), (B) Th1 cells ($CD4^+CXCR3^+CCR6^-$), (C) Th17 cells ($CD4^+CXCR3^-CCR6^+$), (D) total $CD8^+$ cells, (E) $CD8^+$ TEM cells, and (F) $CD8^+$ TEMRA cells ($CCR7^-CD45RA^+$) from the allografts and adjacent native skins. Data are from all three individuals and represented as mean ± SD; statistics by paired t test.

(G) Representative H&E staining (left) and immunofluorescence of $CD4^+$ and $CD8^+$ cells (right) from the allograft and adjacent native skin of the same upper extremity transplant recipient; 200× (scale bars, 100 μm).

See also Figure S3.

characterize the unique features of rejection compared with nonrejection time points in limb transplantation, we characterized circulating T cells during those time points. For the rejection events, we selected blood samples corresponding to a respective Banff grading of 2, 2/3, or 3 skin biopsies from all three individuals. For nonrejection time points, the samples revealed grade 0 or 1 (grade 1 biopsy findings are regarded as non-specific for rejection and are not treated at our institution but monitored closely over time[11]). Compared with nonrejection time points, rejection episodes were characterized by an increase in circulating total $CD8^+$ cells (Figures 3C and 3D), $CD8^+$ TEMRA (Figures 3E and 3F) and $CD4^+$ TEMRA cells (Figures 3G and 3H). Percentages of circulating Treg cells did not change during rejection (Figure 3I), whereas absolute numbers tended to be decreased at rejection time points compared with nonrejection (Figure 3J). In the peripheral blood, we observed an increase in interferon (IFN)-γ-producing $CD4^+$ T cells (Figure 3K) and a decrease in interleukin-4 (IL-4) production by $CD4^+$ T cells during rejection (Figure 3L). No changes were observed in production of IL-17 by circulating $CD4^+$ T cells (Figure 3M) or IFN-γ production by $CD8^+$ T cells (Figure 3N) during rejection events compared with nonrejection.

Expansion of circulating Th1 and TEM cells during rejection

In our cohort, all individuals developed at least one episode of acute cellular rejection within the first 3 years of transplantation (a total of 9 episodes; range, 2–4); about half occurred during the first 3 months after transplantation, whereas the remaining occurred later (>1 year after transplantation). Clinical aspects of the rejection included a maculopapular rash and edema (Figure 3A). Acute cellular rejection was assessed using Banff grading of skin-containing composite tissue,[10] and most clinical rejection episodes were classified as between grades 2 and 3 (Figure 3B). There were no graft failures or recipient deaths. To

Molecular characterization of the graft microenvironment during rejection

To determine the molecular characteristics of the skin tissue associated with rejection, we compared the gene expression profiles of rejection (grades 2–3) and nonrejection (grade 0) events using NanoString technology. Among 770 genes analyzed, 57 genes were differentially expressed during rejection (log2 fold

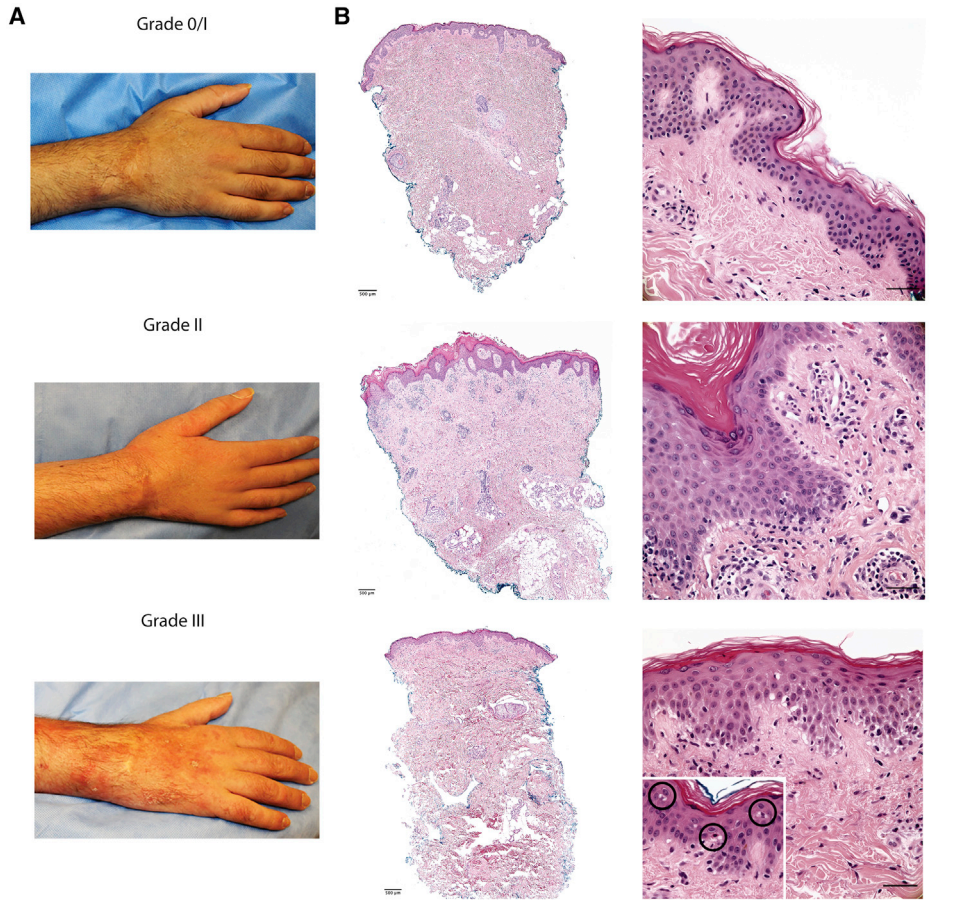

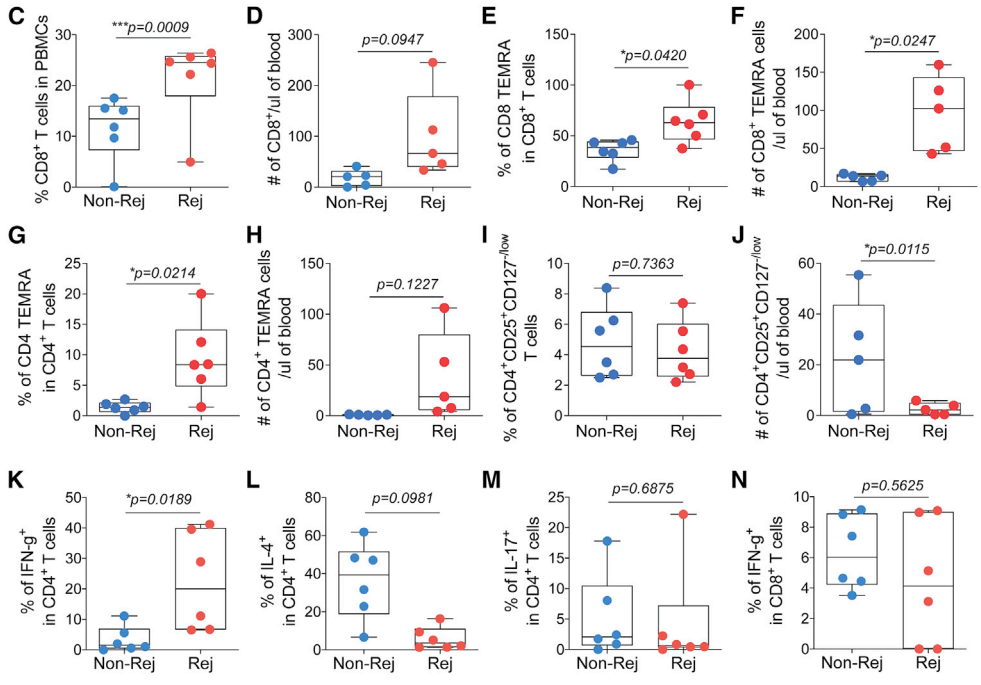

(legend on next page)

change > 2; unadjusted p < 0.01). The differentially expressed genes (DEGs) are displayed in Figure 4A. A principal-component analysis (PCA) was performed for the top 57 DEGs and demonstrated separate clustering of samples with rejection compared with nonrejection events, except for one resolving rejection that clustered with the nonrejection samples (Figure 4B). We used Gene Ontology analysis (GO) to better assess the biological processes that occurred during rejection in the allograft microenvironment. Immune, inflammatory, and chemokine-related responses were strongly associated with the DEGs during the rejection events (Figure 4C). Skin biopsies with rejection had a distinct gene signature compared with nonrejection biopsies.

Rejection is characterized by expression of T cell-recruiting chemokines

From the distinctive gene signature during rejection (Figure 5A), the single most upregulated gene was *CXCL13* (Figure 5B; log2 fold change = 6.1 compared with nonrejection). Following this, many of the top upregulated genes encoded for proteins associated with chemokines and chemokine-mediated signaling (*CCL18*, *CCL17*, *CXCL9*, and *CCL5*; Figure 5B), with CCL18 having a 2-fold increase during rejection. We also found increased gene expression in association with T cell co-stimulation (*TNFRSF4* and *CD28*; Figure 5C) and effector immune molecules (*GZMB*, *GZMA*, *KLRK1*, and *GNLY*; Figure 5E). On the other hand, rejection biopsies also showed increased expression of inhibitory immune checkpoints (*LAG3*, *CTLA4*, and *CD274*; Figure 5D), suggesting that regulatory pathways may be triggered during rejection to counterbalance strong inflammatory responses.

CCL18 enhances recruitment of allogeneic T cells to human skin xenografts

Among the chemokines upregulated during rejection, CCL18 was particularly interesting, based on its primary expression in skin dendritic cells, Langerhans cells, and macrophages[12–14] and its role in recruiting T cells in inflammatory skin conditions such as atopic dermatitis.[5] Therefore, we evaluated the *in vivo* effect of CCL18 and its receptor CCR8 in a humanized skin transplantation model because CCL18 has no murine ortholog (Figure 6A). In this model, we transplanted human foreskins onto genetically immunosuppressed NSG mice and then administered allogeneic PBMCs 4 weeks after the skin transplantation. One week later, animals received daily subcutaneous injections of recombinant human CCL18 or PBS 1× into human skin xenografts for 10 days (Figure 6A). In a subgroup, CCL18-treated animals were administered an anti-CCR8 blocking antibody or isotype control daily starting on the day of PBMCs transfer (Figure 6A). Among the NSG recipients that had received PBMCs, subcutaneous injections of CCL18 into human skin xenografts led to significant macroscopic changes, including tissue shrinkage, discoloration, and dry appearance (Figure 6B). Anti-CCR8 treatment reduced the macroscopic signs of graft rejection induced by CCL18 (Figure 6B). To evaluate whether CCL18 deleterious effects on skin xenografts were dependent on the recipient's immune system, a subgroup of animals was treated with subcutaneous injections of CCL18 or PBS 1× in the absence of PBMCs (Figure 6A). Interestingly, CCL18 treatment did not induce macroscopic changes in skin xenografts of animals that did not receive PBMCs, suggesting that CCL18 effects are dependent on the recipient's immune system (Figure 6C). Histologically, xenografts treated with CCL18 demonstrated reduced $CD31^+$ (vascular endothelium) staining (Figures 6B and 6D) and increased presence of $CD3^+$ cells (Figures 6B and 6E) compared with PBS-injected animals. The anti-CCR8 treatment restored the presence of $CD31^+$ structures (Figures 6B and 6D) and decreased $CD3^+$ cells (Figures 6B and 6E). NSG mice that did not receive PBMCs presented the highest levels of $CD31^+$ vessels that were not affected by CCL18 treatment (Figures 6C and 6D). Xenograft-resident human $CD45^+$ cells were unchanged in CCL18-treated animals that did not receive PBMCs (Figures 6C and 6F). Thus, our data suggest that CCL18 can have major deleterious effects on skin xenografts, which is dependent on the presence of human immune cells.

We next assessed and quantified recruitment of T cells to the skin using T cell extraction protocols and flow cytometry. CCL18 significantly increased the numbers of $CD4^+$ and $CD8^+$ T cells per skin area (Figure 6G and S4). The anti-CCR8 treatment markedly decreased CCL18-induced recruitment of $CD4^+$ and $CD8^+$ T cells (Figure 6G). CCL18 has been shown to recruit cutaneous lymphocyte-associated antigen $(CLA)^+$ T cells to the skin microenvironment.[5] We observed enhanced numbers of CLA^+CD4^+ and CLA^+CD8^+ T cells (Figure 6H) as well as $CCR8^+CD4^+$ and $CCR8^+CD8^+$ T cells (Figure 6I) in skin allografts treated with CCL18. In contrast, CCL18-induced recruitment of CLA^+ and $CCR8^+$ T cells was reduced markedly in anti-CCR8-treated animals (Figures 6H and 6I). Last, we found that CCL18-treated skin was associated with an increased number of Th1, Th2, and Th17 $CD4^+$ T cells compared with vehicle-treated skin, whereas anti-CCR8 treatment inhibited this recruitment (Figure 6J). Our data suggest that CCL18 is an important local chemokine that can increase recruitment of CLA^+ and $CCR8^+$ allo-T cells to human skin xenografts and accelerate graft rejection. CCR8 blockade can substantially abrogate CCL18-induced T cell recruitment and pathogenic effects in skin xenografts.

Figure 3. Clinical and histopathological aspects in upper extremity allograft rejection with correlation to peripheral T cell populations

(A and B) Clinical photographs of an upper extremity transplant recipient and (B) corresponding H&E graft staining during clinical cellular rejection episodes with graft erythema and edema (grades 2–3) compared with mild rejection on surveillance biopsy (grade 1) without significant erythema or edema. Grade 3 rejection retains lymphocytic vasculopathy (bottom right panel) but also shows epithelial apoptosis associated with lymphoid exocytosis (circled in higher magnification, 400×). Left images, 40×; right images, 400× (scale bars, 50 μm).

(C–I) Percentages and (D, F, H, and J) absolute numbers of circulating total $CD8^+$, $CD8^+$ TEMRA, $CD4^+$ TEMRA, and Treg cells at rejection (grades 2–3, n = 6) and nonrejection (grade 0, n = 6) events.

Percentages of (K) IFN-γ^+, (L) IL-4^+, (M) IL-17^+ $CD4^+$ T cells, and (N) IFN-γ^+ $CD8^+$ T cells from peripheral blood at rejection and nonrejection time points.

(C–N) Data are from all three individuals and represented as mean ± SD; statistics by paired t test. Rejection time points included samples from 1 week to 3 years after transplantation and nonrejection time points from 1 month to 4 years after transplantation.

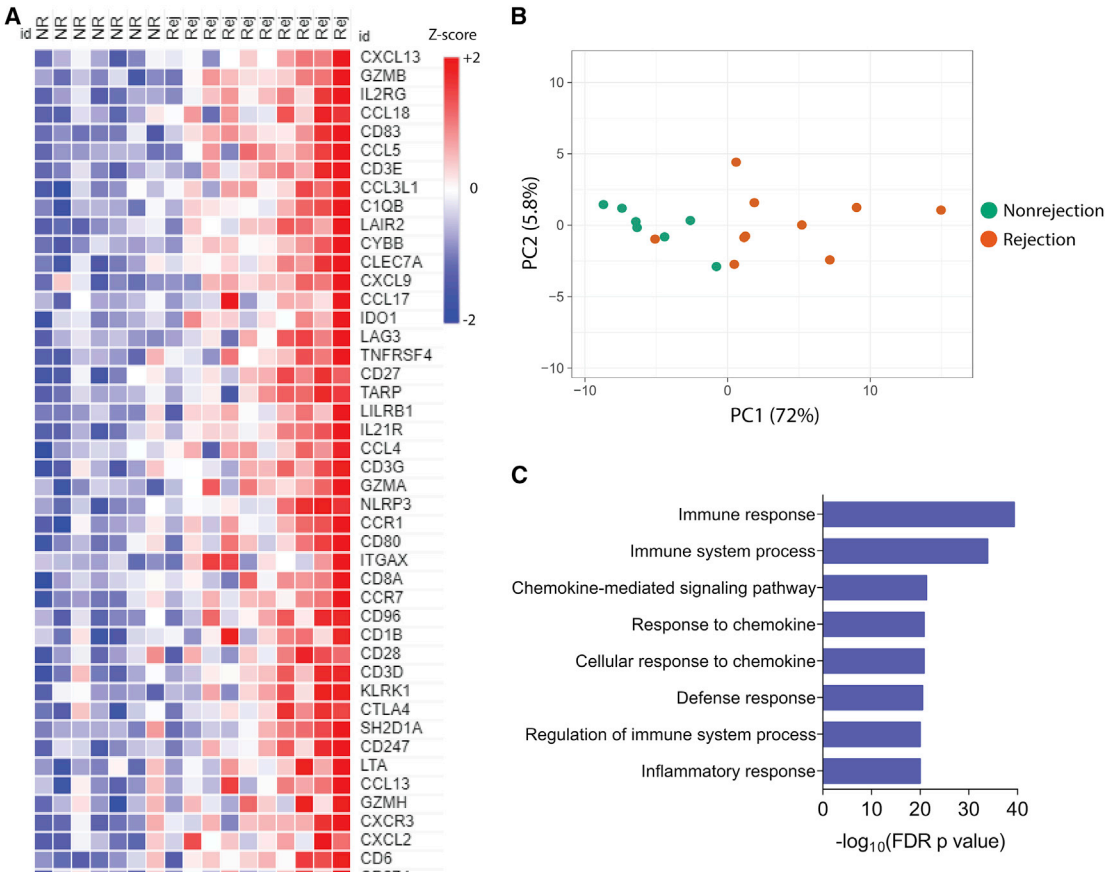

Figure 4. Unique gene expression signature in human upper extremity transplant rejection is associated with chemokines-related genes

(A) Heatmap of the 57 differentially expressed genes (DEGs) in rejection (grades 2–3, n = 10) compared with nonrejection (grades 0–1, n = 7) skin biopsies (log_2 fold change of genes assessed were transformed into *Z* scores).

(B) Unsupervised principal-component analysis of the top 57 DEGs, clustering the samples with rejection compared with nonrejection events, except by one resolving rejection.

(C) Top 8 Gene Ontology (GO) biological process terms enriched among the 57 DEGs in rejection biopsies compared with nonrejection.

Statistics used Fisher's one-tailed test with Benjamini-Hochberg false discovery rate (FDR; p value) for multiple testing correction. For all analyses, rejection biopsies included samples from 1 month to 3 years after transplantation and nonrejection biopsies from 1 month to 4.5 years after transplantation.

DISCUSSION

This study demonstrates that circulating immune cells from limb transplant recipients with no significant graft rejection have predominant Th2 and Treg cell phenotypes that are shifted to Th1 and CD8 responses during rejection. A similar peripheral immune profile was observed in face transplant recipients, as described previously by our group.[15] However, despite the increased circulating Th17 cells over time, we did not observe an increase in Th17 cells infiltrating the allograft during rejection, as demonstrated in face transplant recipients.[15] On one hand, these data suggest that, although skin is the main organ targeted by the immune system in both cohorts of individuals, the dominant effector response appears to differ. On the other hand, chronic rejection has been reported for VCA patients,[16] and this increase in circulating Th17 cells has been associated with chronic graft injury in kidney transplant recipients, whereas reduced Th17 cells have been linked to allograft tolerance.[17,18] In our previous work, focused on face transplant rejection,[19] we found that effector cells represented contributions from

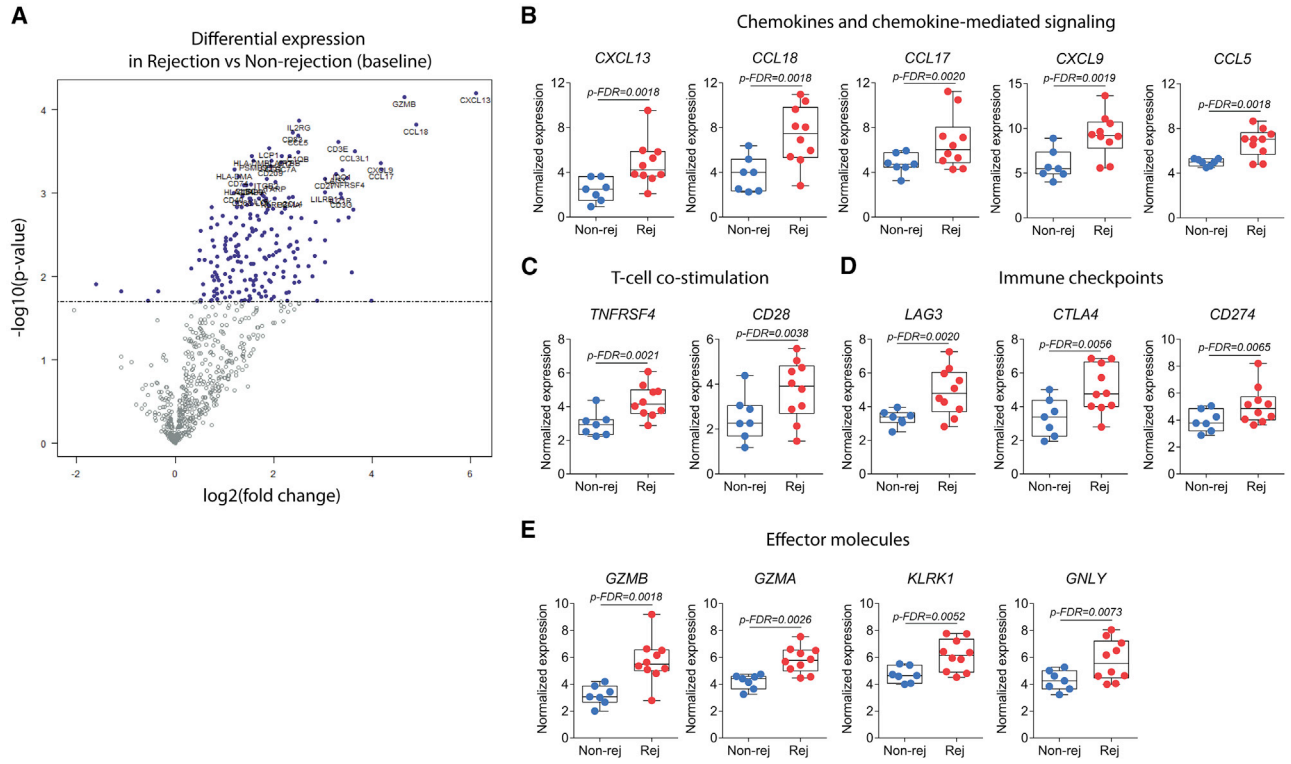

Figure 5. Chemokine-mediated signaling, T cell effector molecules, and immune checkpoints are upregulated in the limb transplant skin microenvironment during rejection

(A) Volcano plot showing DEGs in rejection in relation to nonrejection. Log2 fold change is represented on the x axis, and the y axis displays −log10 of each gene's p value.

(B–E) Normalized expression of genes associated with (B) chemokines and chemokine-mediated signaling, (C) T cell co-stimulation, (D) immune checkpoints, and (E) effector molecules. Boxplots represent mean values with whiskers of maximum and minimum values.

Statistics are represented by FDR p values. For all analyses, rejection biopsies (n = 10; 1 month to 3 years after transplantation) and nonrejection biopsies (n = 7; 1 month to 4.5 years after transplantation).

recipient and donor immune pools. Moreover, donor T cells in rejecting grafts exhibited resident memory phenotypes, implicating local expansion in the transplanted tissue. Targeting events appeared to involve primarily cutaneous venules as well as epithelial domains in the epidermis and hair follicles, where keratinocyte stem cells normally reside.[19] Whether key differences will also emerge in the evolutionary immunopathology between limb and face transplant rejection is a topic in need of further study. However, it is intriguing that Th17 cell pathways are implicated in limb transplantation in the context of data showing that IL-17 can target and activate skin epithelial stem cells through the TRAF4-ERK5 axis.[20]

The skin is an immunologically rich tissue with more than ~1 × 10^6 resident T cells/cm^2 [21] and a diverse and dynamic population of APCs.[22] Seminal studies by Murray[1] have suggested that the skin is the most immunogenic organ. Different skin locations are exposed to diverse external physical and chemical insults that may affect the skin microbiome and the local immune response.[2,23,24] This exposure could cause local non-specific inflammation and mimic alloimmune injury. Through debulking surgeries, we were able to evaluate the local immune profile in the allograft microenvironment and compared it with the adjacent native skin, demonstrating higher numbers of activated T cells in non-rejecting allograft skin. The comparison with adjacent native tissue is crucial because skin from different body areas has significant variation in its immunological content.[25] In agreement with our data, an independent study demonstrated that the cellular infiltrates in skin biopsies from hand transplant recipients were predominantly composed of T cells.[26] Because allograft and adjacent native skin tissues were exposed to the same external factors, our data suggest a more immunologically active environment in the allograft, likely related to continuous local shedding of alloantigens that primarily trigger the adaptive immunity and potentially the innate memory alloresponse.[27] Alternatively, it is possible that leukocyte-endothelium interactions responsible for T cell trafficking and accumulation are altered even in a homograft setting, and this important control situation requires further scrutiny to define this issue.

CCL18 is a chemokine produced by APCs from the dermis and epidermis as well as by keratinocytes, and skin-homing human T cells express CCR8.[28] Increased levels of CCL18 have been linked to atopic dermatitis,[5] psoriasis,[29] allergic contact hypersensitivity,[30] and other human chronic inflammatory diseases.[31] In this report, we found an increase in CCL18 in skin tissue during

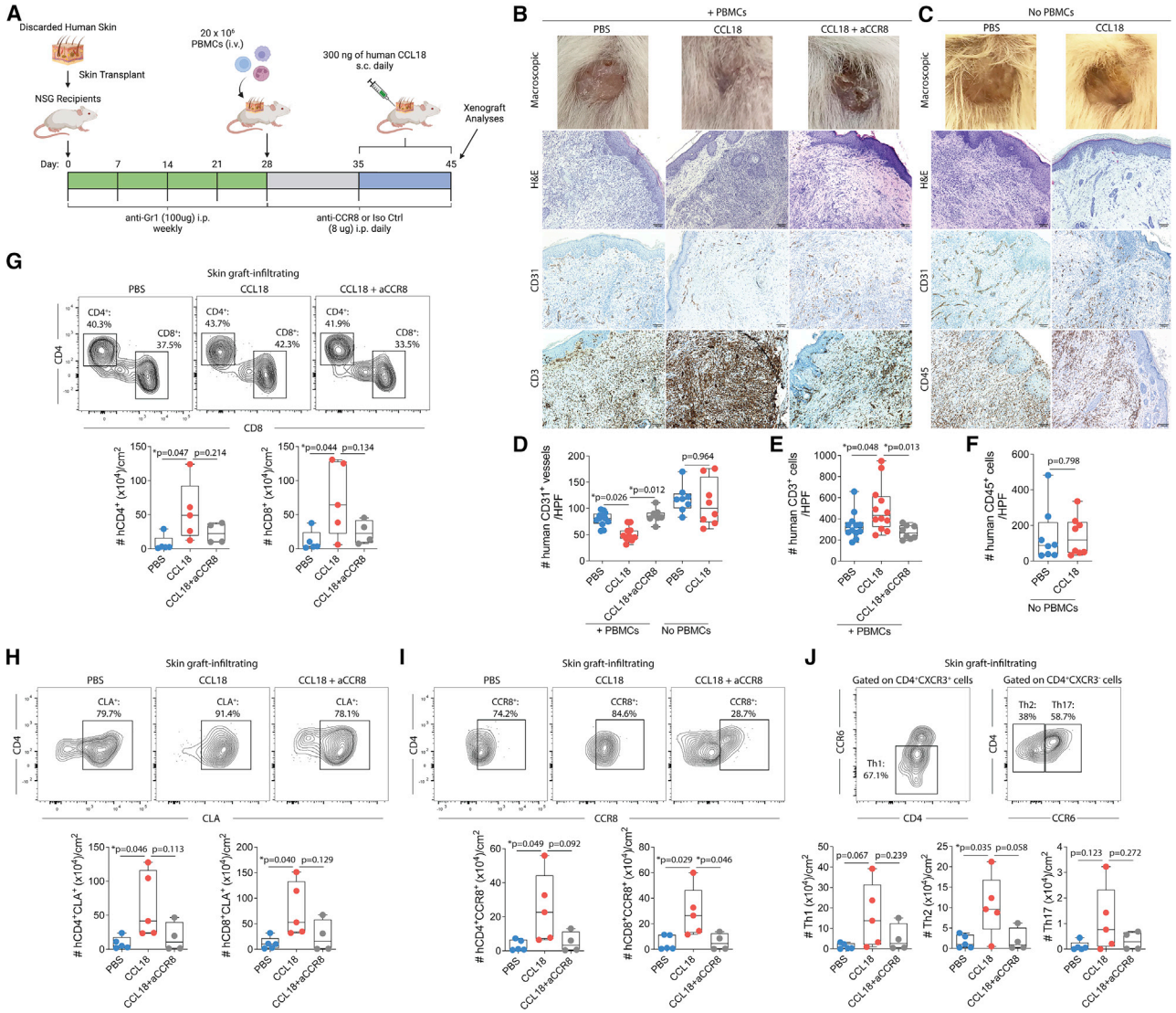

Figure 6. CCL18 attracts human allo-T cells to human skin xenografts

(A and B) Discarded human skin was transplanted into NSG recipient mice. Mice were injected weekly with anti-Gr1 to reduce local inflammation and establish an intact vasculature (A). Twenty-eight days after transplantation, recipients were injected with 20 × 10^6 allo-PBMCs. Seven days thereafter, 300 ng of CCL18 or PBS 1× was injected subcutaneously into the skin xenografts for 10 consecutive days. Recipient animals were treated with anti-CCR8 or isotype control daily. Skin xenografts and peripheral blood were analyzed by histology and flow cytometry on day 45 after transplantation.

(B–D) Representative macroscopic images of skin xenografts, H&E graft staining, and immunohistochemical staining for human CD31, human CD3, or human CD45 after the CCL18 injections into animals (A) injected (B) or not injected (C) with human PBMCs. Shown are absolute counts of human $CD31^+$ vessels.

(E and F) Human $CD3^+$ cells (E) and human $CD45^+$ cells (F) in the skin xenografts, 100×. The number of positive cells was quantified from two representative 400× fields from each transplanted xenograft. Statistics by one-way ANOVA with Tukey's post-test.

(G–J) Representative contour plot and absolute numbers of skin-infiltrating (G) $CD4^+$ and $CD8^+$ cells, (H) skin $CD8^+CLA^+$ and $CD4^+CLA^+$ cells, (I) skin $CD8^+CCR8^+$ and $CD4^+CCR8^+$ cells, and (J) Th1, Th17, and Th2 in PBS-, $CCL18^-$, or $CCL18^+$ anti-CCR8-treated groups that received human PBMCs. All data were normalized by square centimeter of tissue. Data represent a pool of two independent experiments (n = 4–6 animals per group) and are represented as mean ± SD. Statistics by one-way ANOVA with Tukey's post-test.

See also Figure S4.

rejection of VCA. In a humanized skin transplantation model, we demonstrated that local CCL18 injection led to a higher infiltration of T cells in the xenografted human skin. Our results suggest that CCL18 may contribute to VCA rejection by promoting binding of CLA^+ T cells and increasing homing of human memory T cells to the skin.[5] Supporting this possibility, we also observed an increase in skin-infiltrating CLA^+ T cells following CCL18 treatment. These cells have been described to mainly have a memory Th1 cell phenotype[28,32] and collaborate in immune surveillance of healthy skin. When activated T cells infiltrate the skin

allograft, the local inflammatory response may potentiate their effector function and further drive allograft rejection. Among other chemokines present during rejection of extremity transplants, CCL18 may have a unique role in T cell recruitment to the skin in comparison with other organ transplants and thus is a potentially promising selective target for downmodulation of the alloimmune response in VCA transplantation.

Identification of potential biomarkers of rejection is of paramount importance to provide additional tools to diagnose rejection, help physicians in their decision-making about treatment, and develop new therapies. Our group has previously identified serum MMP3 protein as a potential biomarker to stratify VCA recipients according to the severity of rejection.[33,34] Here, besides the increase in CCL18, we also observed an increase in different chemokines, including CXCL9 and CCL5. Along the same lines as our findings, Hautz et al.[26] have demonstrated that markers related to lymphocyte trafficking correlated with the severity of skin rejection in a cohort of five limb transplant recipients. Thus, limb transplant rejection is characterized by upregulation of lymphocyte-attracting chemokines and trafficking markers. These markers comprise potential targets for immunosuppressive drugs. Different chemokines have been reported to be upregulated and have a role during skin allograft rejection responses. CXCL9 and CCL5 have been demonstrated to be upregulated in skin allografts, but not isografts, a few days before rejection.[35] CXCL9, CXCL10, and CCL5 are associated with kidney rejection, and their presence in the urine of transplant recipients is being explored as a rejection biomarker.[36–38] This highlights the potential of chemokines to be used as biomarkers.

Our small number of individuals reflects, in part, the novelty and challenges of extremity transplantation in humans. Despite this, our study employed prospective blood and skin graft collection in combination with high-throughput technologies like NanoString to undercover unique aspects of the rejection process in extremity transplant recipients that may account for its relatively high rejection rate. This comprehensive report of limb transplant recipients is a result of the assembly and curation of a unique biobank with more than 45 time points involving surveillance and rejection episodes. It is now important to validate the pathogenic role of CCL18 and other potential T cell-attracting chemokines in other limb and VCA transplantation cohorts.

Limb transplantation is a clinically feasible procedure for amputees, and use of a solid organ transplantation-based immunosuppressive regimen has yielded good short/medium-term graft outcomes. Nonetheless, the high frequency of cellular rejection is a concerning long-term barrier. Development of novel biomarkers in larger cohorts and less toxic, narrowly targeted skin-specific immunosuppression strategies are critical to advance the field.

Limitations of the study

Limitations of our study include its single-center nature and the small number of individuals evaluated, limiting major extrapolations. Our findings need to be validated in other limb and VCA cohorts from different centers. We also acknowledged that, although NanoString is a useful tool, its detection capacity is limited to fewer than 1,000 transcripts. More comprehensive analyses, like single-cell RNA sequencing, could have identified other transcriptional pathways unique to the rejection process in limb transplant recipients. Finally, the results from the humanized skin transplantation are limited by the variability found in this model and the inability to fully recapitulate the complexity of the human immune system.

STAR★METHODS

Detailed methods are provided in the online version of this paper and include the following:

- KEY RESOURCES TABLE
- RESOURCE AVAILABILITY
  - Lead contact
  - Materials availability
  - Data and code availability
- EXPERIMENTAL MODEL AND SUBJECT DETAILS
  - Upper extremities transplant subjects and study approval
  - Patients' immunosuppression
  - Humanized skin transplant model
- METHODS DETAILS
  - Isolation and quantification of skin cells
  - Flow cytometry
  - Histology and immunofluorescence staining
  - Immunohistochemistry
  - RNA extraction
  - NanoString nCounter assay for mRNA gene expression assay
- QUANTIFICATION AND STATISTICAL ANALYSIS
- ADDITIONAL RESOURCES

SUPPLEMENTAL INFORMATION

Supplemental information can be found online at https://doi.org/10.1016/j.xcrm.2022.100559.

ACKNOWLEDGMENTS

L.V.R. received support from the Department of Defense (RT190059, award W81XWH-20-1-0758). S.G.T. receives salary support from the Office of the Assistant Secretary of Defense for Health Affairs under the Reconstructive Transplant Research Program – Qualitative Research Award under award W81XWH-17-1-0400 and the Joint Program Committee 8/Clinical and Rehabilitative Medicine Research Program Extremity Regeneration Technology/Therapeutic Development Award under award W81XWH-16-2-0067. R.A.C. was supported by the Department of Defense (awards RT150073 and RT170025). Opinions, interpretations, conclusions, and recommendations are those of the author and are not necessarily endorsed by the Department of Defense. T.J.B. was the recipient of an American Heart Association postdoctoral fellowship (20POST35210659). B.K. was the recipient of the Plastic Surgery Foundation research fellowship grant.

AUTHOR CONTRIBUTIONS

T.J.B. and L.V.R. conceived the study and wrote the manuscript. T.J.B. performed flow cytometry, NanoString, animal experiments, and analyses. P.A., G.F.M., and G.C.L. performed the patient histology experiments and analyses. B.K. collected the clinical data. R.B.G., M.L.-F., and B.T.A. assisted T.J.B. with the animal transplants. D.G. performed the xenograft histology. B.P., G.F.M., R.A.C., S.A.I., G.C.L., and S.G.T. helped interpret the results and edited the manuscript. All authors reviewed the manuscript critically for important intellectual content and gave final approval of the version to be submitted.

DECLARATION OF INTERESTS

The authors declare no competing interests.

INCLUSION AND DIVERSITY

One or more of the authors of this paper self-identifies as an underrepresented ethnic minority in science. One or more of the authors of this paper self-identifies as a member of the LGBTQ+ community.

Received: April 15, 2021
Revised: January 14, 2022
Accepted: February 12, 2022
Published: March 15, 2022

REFERENCES

1. Murray, J.E. (1971). Organ transplantation (skin, kidney, heart) and the plastic surgeon. Plast. Reconstr. Surg. *47*, 425–431.
2. Kollar, B., Pomahac, B., and Riella, L.V. (2019). Novel immunological and clinical insights in vascularized composite allotransplantation. Curr. Opin. Organ Transpl. *24*, 42–48.
3. Hein, R.E., Ruch, D.S., Klifto, C.S., Leversedge, F.J., Mithani, S.K., Pidgeon, T.S., Richard, M.J., and Cendales, L.C. (2019). Hand transplantation in the United States: a review of the organ procurement and transplantation network/united network for organ sharing database. Am. J. Transpl. *20*, 1417–1423.
4. Islam, S.A., Ling, M.F., Leung, J., Shreffler, W.G., and Luster, A.D. (2013). Identification of human CCR8 as a CCL18 receptor. J. Exp. Med. *210*, 1889–1898.
5. Günther, C., Bello-Fernandez, C., Kopp, T., Kund, J., Carballido-Perrig, N., Hinteregger, S., Fassl, S., Schwärzler, C., Lametschwandtner, G., Stingl, G., et al. (2005). CCL18 is expressed in atopic dermatitis and mediates skin homing of human memory T cells. J. Immunol. *174*, 1723–1728.
6. Park, C.O., Lee, H.J., Lee, J.H., Wu, W.H., Chang, N.S., Hua, L., Lee, M.G., and Lee, K.H. (2008). Increased expression of CC chemokine ligand 18 in extrinsic atopic dermatitis patients. Exp. Dermatol. *17*, 24–29.
7. Vieyra-Garcia, P., Crouch, J.D., O'Malley, J.T., Seger, E.W., Yang, C.H., Teague, J.E., Vromans, A.M., Gehad, A., Win, T.S., Yu, Z., et al. (2019). Benign T cells drive clinical skin inflammation in cutaneous T cell lymphoma. JCI Insight *4*, e124233.
8. Weaver, C.T., Elson, C.O., Fouser, L.A., and Kolls, J.K. (2013). The Th17 pathway and inflammatory diseases of the intestines, lungs, and skin. Annu. Rev. Pathol. Mech. Dis. *8*, 477–512.
9. Liu, T., Li, S., Ying, S., Tang, S., Ding, Y., Li, Y., Qiao, J., and Fang, H. (2020). The IL-23/IL-17 pathway in inflammatory skin diseases: from bench to bedside. Front. Immunol. *11*, 2971.
10. Cendales, L.C., Kanitakis, J., Schneeberger, S., Burns, C., Ruiz, P., Landin, L., Remmelink, M., Hewitt, C.W., Landgren, T., Lyons, B., et al. (2008). The Banff 2007 working classification of skin-containing composite tissue allograft pathology. Am. J. Transplant. *8*, 1396–1400.
11. Tasigiorgos, S., Kollar, B., Turk, M., Perry, B., Alhefzi, M., Kiwanuka, H., Nizzi, M.-C., Marty, F.M., Chandraker, A., Tullius, S.G., et al. (2019). Five-Year follow-up after face transplantation. N. Engl. J. Med. *380*, 2579–2581.
12. Günther, C., Zimmermann, N., Berndt, N., Grosser, M., Stein, A., Koch, A., and Meurer, M. (2011). Up-regulation of the chemokine CCL18 by macrophages is a potential immunomodulatory pathway in cutaneous T-cell lymphoma. Am. J. Pathol. *179*, 1434–1442.
13. He, H., Suryawanshi, H., Morozov, P., Gay-Mimbrera, J., Del Duca, E., Kim, H.J., Kameyama, N., Estrada, Y., Der, E., Krueger, J.G., et al. (2020). Single-cell transcriptome analysis of human skin identifies novel fibroblast subpopulation and enrichment of immune subsets in atopic dermatitis. J. Allergy Clin. Immunol. *145*, 1615–1628.
14. Reynolds, G., Vegh, P., Fletcher, J., Poyner, E.F.M., Stephenson, E., Goh, I., Botting, R.A., Huang, N., Olabi, B., Dubois, A., et al. (2021). Developmental cell programs are co-opted in inflammatory skin disease. Science *371*, eaba6500.
15. Borges, T.J., O'Malley, J.T., Wo, L., Murakami, N., Smith, B., Azzi, J., Tripathi, S., Lane, J.D., Bueno, E.M., Clark, R.A., et al. (2016). Codominant role of interferon-γ– and interleukin-17–producing T cells during rejection in full facial transplant recipients. Am. J. Transpl. *16*, 2158–2171.
16. Krezdorn, N., Lian, C.G., Wells, M., Wo, L., Tasigiorgos, S., Xu, S., Borges, T.J., Frierson, R.M., Stanek, E., Riella, L.V., et al. (2019). Chronic rejection of human face allografts. Am. J. Transpl. *19*, 1168–1177.
17. Chung, B.H., Kim, K.W., Kim, B.-M., Doh, K.C., Cho, M.-L., and Yang, C.W. (2015). Increase of Th17 cell phenotype in kidney transplant recipients with chronic allograft dysfunction. PLoS One *10*, e0145258.
18. Nova-Lamperti, E., Romano, M., Christakoudi, S., Runglall, M., McGregor, R., Mobillo, P., Kamra, Y., Tsui, T.-L., Norris, S., John, S., et al. (2018). Reduced TCR signaling contributes to impaired Th17 responses in tolerant kidney transplant recipients. Transplantation *102*, e10–e17.
19. Lian, C.G., Bueno, E.M., Granter, S.R., Laga, A.C., Saavedra, A.P., Lin, W.M., Susa, J.S., Zhan, Q., Chandraker, A.K., Tullius, S.G., et al. (2014). Biomarker evaluation of face transplant rejection: association of donor T cells with target cell injury. Mod. Pathol. *27*, 788–799.
20. Wu, L., Chen, X., Zhao, J., Martin, B., Zepp, J.A., Ko, J.S., Gu, C., Cai, G., Ouyang, W., Sen, G., et al. (2015). A novel IL-17 signaling pathway controlling keratinocyte proliferation and tumorigenesis via the TRAF4-ERK5 axis. J. Exp. Med. *212*, 1571–1587.
21. Clark, R.A., Chong, B., Mirchandani, N., Brinster, N.K., Yamanaka, K.-I., Dowgiert, R.K., and Kupper, T.S. (2006). The vast majority of CLA+ T cells are resident in normal skin. J. Immunol. *176*, 4431–4439.
22. Heath, W.R., and Carbone, F.R. (2013). The skin-resident and migratory immune system in steady state and memory: innate lymphocytes, dendritic cells and T cells. Nat. Immunol. *14*, 978–985.
23. Etra, J.W., Shores, J.T., Sander, I.B., Brandacher, G., and Lee, W.P.A. (2020). Trauma-induced rejection in vascularized composite allotransplantation. Ann. Surg. *271*, e113–e114.
24. Lopdrup, R.G., Turk, M., Win, T.S., Marty, F.M., Molway, D., Tullius, S.G., Pomahac, B., and Talbot, S.G. (2017). Seasonal variability precipitating hand transplant rejection? Transplantation *101*, e313.
25. Tong, P.L., Roediger, B., Kolesnikoff, N., Biro, M., Tay, S.S., Jain, R., Shaw, L.E., Grimbaldeston, M.A., and Weninger, W. (2015). The skin immune atlas: three-dimensional analysis of cutaneous leukocyte subsets by multiphoton microscopy. J. Invest. Dermatol. *135*, 84–93.
26. Hautz, T., Zelger, B., Grahammer, J., Krapf, C., Amberger, A., Brandacher, G., Landin, L., Pratschke, J., Margreiter, R., and Schneeberger, S. (2010). Molecular markers and targeted therapy of skin rejection in composite tissue allotransplantation. Am. J. Transpl. *10*, 1200–1209.
27. Dai, H., Lan, P., Zhao, D., Abou-Daya, K., Liu, W., Chen, W., Friday, A.J., Williams, A.L., Sun, T., Chen, J., et al. (2020). PIRs mediate innate myeloid cell memory to nonself MHC molecules. Science *368*, 1122–1127.
28. Schaerli, P., Ebert, L., Willimann, K., Blaser, A., Roos, R.S., Loetscher, P., and Moser, B. (2004). A skin-selective homing mechanism for human immune surveillance T Cells. J. Exp. Med. *199*, 1265–1275.
29. Kim, H.O., Cho, S.I., Chung, B.Y., Ahn, H.K., Park, C.W., and Lee, C.H. (2012). Expression of CCL1 and CCL18 in atopic dermatitis and psoriasis. Clin. Exp. Dermatol. *37*, 521–526.
30. Goebeler, M., Trautmann, A., Voss, A., Bröcker, E.B., Toksoy, A., and Gillitzer, R. (2001). Differential and sequential expression of multiple chemokines during elicitation of allergic contact hypersensitivity. Am. J. Pathol. *158*, 431–440.
31. Schutyser, E. (2005). Involvement of CC chemokine ligand 18 (CCL18) in normal and pathological processes. J. Leukoc. Biol. *78*, 14–26.
32. Colantonio, L., Iellem, A., Sinigaglia, F., and D'Ambrosio, D. (2002). Skin-homing CLA+ T cells and regulatory CD25+ T cells represent major

subsets of human peripheral blood memory T cells migrating in response to CCL1/I-309. Eur. J. Immunol. *32*, 3506–3514.

33. Kollar, B., Shubin, A., Borges, T.J., Tasigiorgos, S., Win, T.S., Lian, C.G., Dillon, S.T., Gu, X., Wyrobnik, I., Murphy, G.F., et al. (2018). Increased levels of circulating MMP3 correlate with severe rejection in face transplantation. Sci. Rep. *8*, 14915.

34. Kollar, B., Uffing, A., Borges, T.J., Shubin, A.V., Aoyama, B.T., Dagot, C., Haug, V., Kauke, M., Safi, A.F., Talbot, S.G., et al. (2019). MMP3 is a noninvasive biomarker of rejection in skin-bearing vascularized composite allotransplantation: a multicenter validation study. Front. Immunol. *10*, 2771.

35. Watarai, Y., Koga, S., Paolone, D.R., Engeman, T.M., Tannenbaum, C., Hamilton, T.A., and Fairchild, R.L. (2000). Intraallograft chemokine RNA and protein during rejection of MHC-matched/multiple minor histocompatibility-disparate skin grafts. J. Immunol. *164*, 6027–6033.

36. Hricik, D.E., Nickerson, P., Formica, R.N., Poggio, E.D., Rush, D., Newell, K.A., Goebel, J., Gibson, I.W., Fairchild, R.L., Riggs, M., et al. (2013). Multicenter validation of urinary CXCL9 as a risk-stratifying biomarker for kidney transplant injury. Am. J. Transpl. *13*, 2634–2644.

37. Ho, J., Schaub, S., Wiebe, C., Gao, A., Wehmeier, C., Koller, M.T., Hirsch, H.H., Hopfer, H., Nickerson, P., and Hirt-Minkowski, P. (2018). Urinary CXCL10 chemokine is associated with alloimmune and virus compartment-specific renal allograft inflammation. Transplantation *102*, 521–529.

38. Kaminski, M.M., Alcantar, M.A., Lape, I.T., Greensmith, R., Huske, A.C., Valeri, J.A., Marty, F.M., Klämbt, V., Azzi, J., Akalin, E., et al. (2020). A CRISPR-based assay for the detection of opportunistic infections post-transplantation and for the monitoring of transplant rejection. Nat. Biomed. Eng. *4*, 601–609.

39. Christofidou-Solomidou, M., Longley, B.J., Whitaker-Menezes, D., Albelda, S.M., and Murphy, G.F. (1997). Human skin/SCID mouse chimeras as an in vivo model for human cutaneous mast cell hyperplasia. J. Invest. Dermatol. *109*, 102–107.

40. Watanabe, R., Gehad, A., Yang, C., Scott, L.L., Teague, J.E., Schlapbach, C., Elco, C.P., Huang, V., Matos, T.R., Kupper, T.S., et al. (2015). Human skin is protected by four functionally and phenotypically discrete populations of resident and recirculating memory T cells. Sci. Transl. Med. *7*, 279ra39.

41. Racki, W.J., Covassin, L., Brehm, M., Pino, S., Ignotz, R., Dunn, R., Laning, J., Graves, S.K., Rossini, A.A., Shultz, L.D., et al. (2010). NOD-scid IL2r-gamma(null) mouse model of human skin transplantation and allograft rejection. Transplantation *89*, 527–536.

42. Borges, T.J., Murakami, N., Machado, F.D., Murshid, A., Lang, B.J., Lopes, R.L., Bellan, L.M., Uehara, M., Antunes, K.H., Pérez-Saéz, M.J., et al. (2018). March1-dependent modulation of donor MHC II on CD103+ dendritic cells mitigates alloimmunity. Nat. Commun. *9*, 3482.

43. Metsalu, T., and Vilo, J. (2015). ClustVis: a web tool for visualizing clustering of multivariate data using principal component analysis and heatmap. Nucleic Acids Res. *43*, W566–W570.

44. Mi, H., Muruganujan, A., Ebert, D., Huang, X., and Thomas, P.D. (2019). PANTHER version 14: more genomes, a new PANTHER GO-slim and improvements in enrichment analysis tools. Nucleic Acids Res. *47*, D419–D426.

STAR★METHODS

KEY RESOURCES TABLE

REAGENT	SOURCE	IDENTIFIER
Biological Samples		
PBMCs from limb transplant patients	This study (BWH)	N/A
Punch skin biopsies from limb transplant patients	This study (BWH)	N/A
Human discarded foreskin specimens	This study (BWH)	N/A
PBMCs from healthy volunteers	This study (BWH and MGH)	N/A
Experimental models		
NSG (*M. musculus*)	Jackson Lab	NOD.Cg-Prkdc^{scid} Il2rg^{tm1Wjl}/SzJ
Antibodies		
APC/Cyanine7 anti-human CD4	Biolegend	Clone OKT4; RRID: AB_2687202
PerCP/Cyanine5.5 anti-human CD4	Biolegend	Clone OKT4; RRID: AB_1186122
PerCP/Cy5.5 anti-human CD127	Biolegend	Clone A019D5; RRID: AB_10900253
FITC anti-human CD185 (CXCR5)	Biolegend	Clone J252D4; RRID: AB_2561896
PE/Cyanine7 anti-human CD279 (PD-1)	Biolegend	Clone EH12.2H7; RRID: AB_2159325
APC anti-human FOXP3	ThermoFisher	Clone 236A/E7; RRID: AB_10804651
Brilliant Violet 510^{TM} anti-human CD8	Biolegend	Clone SK1; RRID: AB_2564623
BUV737 anti-human CD8	BD Biosciences	Clone SK1; RRID: AB_2870085
APC anti-human CD45RA	BD Biosciences	Clone HI100; RRID: AB_314416
APC anti-human CD45RA	Biolegend	Clone HI100; RRID: AB_314416
PE anti-human CD45RA	Biolegend	Clone HI100; RRID: AB_314412
FITC anti-human CD183 (CXCR3)	Biolegend	Clone G025H7; RRID: AB_10983066
PerCP/Cyanine5.5 anti-human CD197 (CCR7)	Biolegend	Clone G043H7; RRID: AB_10915275
PE/Cyanine7 anti-human CD196 (CCR6)	Biolegend	Clone G034E3; RRID: AB_10916518
APC anti-human CD196 (CCR6)	Biolegend	Clone G034E3; RRID: AB_10915987
PE anti-mouse/human B220	Biolegend	Clone RA3-6B2; RRID: AB_312992
APC-eFluor 780 anti-human IFN-gamma	Thermo Fisher	Clone 4S.B3; RRID: AB_10853011
PE anti-human IL-17A	Thermo Fisher	Clone eBio64DEC17; RRID: AB_1724136
PE anti-human CD25	BD Biosciences	Clone M-A251; RRID: AB_2561860
PE/Cy7 anti-human CD45 Antibody	BD Biosciences	Clone HI30; RRID: AB_314403
PerCP/Cyanine5.5 anti-human/mouse CLA	Biolegend	Clone HECA-452; RRID: AB_2565765
APC anti-human CD198 (CCR8)	Biolegend	Clone L263G8; RRID: AB_2820018
Pacific Blue anti-human CD19	Biolegend	Clone HIB19; RRID: AB_2073118
Brilliant Violet 605^{TM} anti-human CD3	Biolegend	Clone OKT3; RRID: AB_2565824
PE anti-human FOXP3	Biolegend	Clone 206D; RRID: AB_492986
Purified anti-human CCR8	Biolegend	Clone L263G8; RRID: AB_2562613
Purified mouse IgG2a, κ	Biolegend	Clone MOPC-173; RRID: AB_326546
InVivoMAb anti-mouse Ly6G/Ly6C (Gr-1)	Bio X Cell	Clone RB6-8C5
FcR Blocking Reagent, human	Miltenyi	Cat # 130-059-901; RRID: AB_2892112
Rabbit-anti-human CD4, polyclonal	Novus Biologicals	Cat # NBP1-19371; RRID: AB_1641682
Mouse anti-human CD8 alpha	Abcam	Clone C8/144B; RRID: AB_1280806
Goat anti-rabbit IgG Antibody (H+L), Biotinylated	Vector Labs	Cat # BA-1000-1.5
Horse anti-mouse IgG Antibody (H+L), Biotinylated	Vector Labs	Cat # BA-2000-1.5
Rabbit anti-CD3	Roche	Clone 2GV6
Rabbit Polyclonal Anti-CD31	Abcam	Cat # ab28364; RRID: AB_726362
Rabbit anti-human CD45	Cell Signaling	Cat # 13917S; RRID: AB_2750898
Rabbit anti-mouse CD45	Cell Signaling	Cat # 70257S; RRID: AB_2799780

(*Continued on next page*)

Continued

REAGENT	SOURCE	IDENTIFIER
Critical commercial assays		
nCounter® PanCancer Immune Profiling Panel	NanoString	Cat # XT-CSO-HIP1-12
Chemicals, peptides, and recombinant proteins		
Fixable Viability Dye eFluor 780	Thermo Fisher	Cat # 65-0865-14
Zombie NIR Fixable Viability Kit	Biolegend	Cat # 423106
LIVE/DEAD™ Fixable Blue Dead Cell Stain Kit	Thermo Fisher	Cat # L34961
Foxp3/Transcription Factor Staining Buffer Set	ThermoFisher	Cat # 00-5523-00
Phorbol 12-myristate 13-acetate (PMA) and Ionomycin	Biolegend	Cat # 423301
GolgiStop	BD Biosciences	Cat # 554724
Recombinant human CCL18	Peprotech	Cat # 300-34
RPMI 1640 Medium with L-Glutamine	Lonza	Cat # 12-702Q
BenchMark Fetal Bovine Serum	GeminiBio	Cat # 100-106
Penicillin-Streptomycin Solution	Corning	Cat # 30-002-CI
Collagenase type I	Thermo Fisher	Cat # 17100017
DNase I	Thermo Fisher	Cat # 18047019
AccuCheck Counting Beads	Thermo Fisher	Cat # PCB100
Target Retrieval Solution, Citrate pH 6	Agilent Dako	Cat # S236984-2
Streptavidin, Alexa Fluor 546 conjugate	Thermo Fisher	Cat # S11225
Streptavidin, Alexa Fluor 647 conjugate	Thermo Fisher	Cat # S21374
ProLong Gold Antifade Mountant with DAPI	Thermo Fisher	Cat # P36931
RNeasy FFPE Kit	Qiagen	Cat # 73504
nCounter Standard Master Kit	NanoString	Cat # NAA-AKIT-01
Software and algorithms		
FlowJo v 10.7.1	FlowJo	N/A
Graphpad Prism v9.0	GraphPad Software	N/A
nSolver Analysis Software v4.0.70	Nanostring	N/A
Morpheus	https://software.broadinstitute.org/morpheus	N/A
ClustVis v2.0	https://biit.cs.ut.ee/clustvis/	Metsalu et al., 2015
PANTHER v16.0	http://pantherdb.org	Mi et al., 2019
ZEN 2012 v1.1.2.0	ZEISS	N/A
Illustrator v26.0.1	Adobe	N/A
Photoshop v23.1.0	Adobe	N/A
ImageJ v2.0.0-rc-69/1.52p	https://imagej.net	N/A
Other		
Axio Imager.M2	ZEISS	N/A
Fortessa X-20	BD Biosciences	N/A
VENTANA BenchMark Stain System	Roche	N/A
nCOUNTER FLEX	NanoString	N/A

RESOURCE AVAILABILITY

Lead contact

Further information and requests for resources and reagents should be directed to and will be fulfilled by the lead contact (Iriella@mgh.harvard.edu).

Materials availability

This study did not generate new unique reagents.

Data and code availability

All data reported in this paper will be shared by the lead contact upon request. This paper does not report the original code. Any additional information required to reanalyze the data reported in this paper is available from the lead contact upon request.

EXPERIMENTAL MODEL AND SUBJECT DETAILS

Upper extremities transplant subjects and study approval

Three patients who received upper extremities transplants at the Brigham and Women's Hospital were included in the study. All patients provided written informed consent to participate in the clinical trial (ClinicalTrials.gov NCT01293214) for upper extremities transplantation, as approved by the Human Research Committee at Brigham and Women's Hospital (2009P001719). Before participation, patients were evaluated by our multidisciplinary team. Donors and recipients were matched according to sex, skin color, and ABO compatibility, in addition to a negative T and B cell cytotoxic crossmatch. Demographic details are displayed in Table 1. Patients were followed weekly during the first 4–6 weeks after transplantation and if stable, clinical visits were further spaced to every 2 weeks, every month, and then every 3 months. After the first year of transplantation, the clinical visits were scheduled semiannually.

Patients' immunosuppression

All patients received mycophenolate mofetil (1,000 mg), methylprednisolone (500 mg), and rabbit anti-thymocyte globulin (1.5 mg/kg/day × 4 days) for induction therapy starting at the time of transplantation. Maintenance immunosuppression consisted of mycophenolate mofetil (initially 1,000 mg twice daily, and reduced to 500–750 mg twice daily in long-term), tacrolimus (adjusted to achieve target levels of 10–15 ng/mL in the first 6 months, followed by 8–12 ng/mL up to 1 year and 6–10 ng/mL thereafter), and prednisone taper (down to 20 mg on day 5, and 5–7.5 mg in long-term) (Table 1). Prednisone withdrawal was attempted in Patient 1, but due to the higher occurrence of acute rejection episodes during winter months, low dose prednisone (5 mg) was seasonally reinitiated.[24] Perioperative antibacterial prophylaxis consisted of vancomycin and cefazolin and was modified according to perioperative findings. All patients received trimethoprim–sulfamethoxazole and valganciclovir prophylaxis against *Pneumocystis jirovecii* and cytomegalovirus, respectively, for $\geq$6 months. In the presence of clinical acute cellular rejection, patients were treated with pulse solumedrol 500 mg/day for 3 days, followed by a taper. Acute rejection episodes with no clinical signs were treated with an increase in maintenance immunosuppression and closely followed. Topical steroids or tacrolimus were also used in a few cases as adjuvant therapy. In case of no response, further T cell–depletion therapy (rabbit anti-thymocyte globulin, alemtuzumab) was attempted.

Humanized skin transplant model

Six-to-eight weeks-old NSG recipient mice were transplanted with a full-thickness (1 cm^2 section) human foreskin xenograft on dorsum using a sterile monofilament, non-absorbable suture, as previously described by a member of our group (GFM[39]). Foreskins were used because they have fewer resident T cells.[40] Human skin tissues were obtained as discarded tissue from plastic surgery (MGB IRB 2016P001844 and 2019P002424). Transplanted animals were treated weekly with 100 μg of an anti-Gr1 antibody (clone RB6-8C5, Bio X Cell) to reduce local cellular infiltration, improve wound healing, and establish an intact human vasculature.[41] Four weeks later, each mouse was i.v. injected with 20 × 106 PBMCs from a different donor (allo-PBMCs). One week later, 300 ng of CCL18 (in 100 μL of sterile PBS 1×; purchased from Peprotech) was subcutaneously injected, under the skin allograft for ten consecutive days. The control group received sterile PBS 1× alone. Some animals were intraperitoneally treated with 8 μg anti-human CCR8 (clone L263G8, Biolegend) or mouse IgG2a, κ isotype control (clone MOPC-173, Biolegend). Skin xenografts were daily monitored for signs of rejection, primarily change in color and necrosis. Skin allografts and peripheral blood were harvested for analyses on day 17 after the PBMCs adoptive transfer. All animals were housed following the Institutional Animal Care and Use Committee (IACUC) and National Institutes of Health (NIH) Animal Care guidelines. The Mass General Brigham IACUC approved all experiments (protocol number 2016N000250 and 2020N000125).

METHODS DETAILS

Isolation and quantification of skin cells

Immune cells from debulking surgeries or skin xenografts were isolated, as described previously.[42] After harvesting, skin tissues were recovered overnight in RPMI media (Lonza) supplemented with 20% FBS (GeminiBio), 100 mM L-glutamine and ×1 penicillin/streptomycin at 4°C. After that, the tissues were minced into small pieces in 10% FCS-supplemented RPMI, followed by incubation in Collagenase type I (Thermo Fisher, 0.2%) and DNase I (Thermo Fisher, 30 Kunitz Units/mL) at 37°C for 2 h with shaking (350 rpm). Cells were passed through 70 μm cell-strainer, washed and recovered in RPMI media (Lonza) supplemented with 20% FBS, 100 mM L-glutamine and penicillin/streptomycin for 4h or overnight at 37°C. We quantified the total skin cell numbers using fluorescent AccuCheck Counting Beads (Invitrogen) by flow cytometry. Each skin sample had its area calculated and all data were normalized by skin area (in cm^2).

Flow cytometry

We stained PBMCs, skin cells from debulking surgeries or xenografts for flow cytometry. PBMCs from different time points from the same patient were thawed, washed and stained on the same day to avoid variability. Over time analysis displayed in Figure 1 included

samples from pre-transplant, 24 h, 1 week, 3-, 6- and 12-months post-transplant. Rejection time points included samples from 1 week to 3 years post-transplantation, and nonrejection time points from 1 month to 4 years post-transplantation. Thawed PBMCs and recovered skin cells were Fc-blocked (Miltenyi) for 20 min before staining for surface markers for 30 min in FACS buffer (2% FBS in PBS 1x) on ice. Intracellular staining was performed using the Fixation/Permeabilization Kit (Thermo Fisher). For PBMC analyses over time and during rejection episodes, we used the following anti-human antibodies: anti-CD4 (1:100), anti-CD8 (1:100), anti-CD45RA (1:100), anti-CCR7 (1:20), anti-CD25 (1:66), anti-CD127 (1:50), anti-CXCR5 (1:100), anti-PD-1 (1:400), anti-CXCR3 (1:50), anti-CCR6 (1:40), anti-IFN-γ (1:40), anti-IL-4 (1:40) and IL-17A (1:40). For cytokine detection, cell suspensions were incubated for 6 h with 50 ng/mL of phorbol 12-myristate 13-acetate (PMA) plus 500 ng/mL ionomycin (Biolegend), and GolgiStop (BD Biosciences) in 10% FBS-RPMI, followed by surface staining, permeabilization, and intracellular staining. For the experiments with NSG mice, we used the following anti-human antibodies: anti-CD45 (1:100), anti-CD3 (1:100), anti-CD4 (1:100), anti-CD8 (1:50), anti-CD19 (1:200), anti-CLA (1:33), anti-CCR8 (1:33), anti-CXCR3 (1:50) and anti-CCR6 (1:40). Stained cells were analyzed on a FACS Canto II flow cytometer (BD Biosciences) with FACSDiva software (BD Biosciences). Data were analyzed with FlowJo software (TreeStar). Viable cells were selected based on the staining with Fixable Viability Dye eFluor 780 (Thermo Fisher), Zombie NIR Fixable Viability Kit (Biolegend) or LIVE/DEAD Fixable Blue Dead Cell Stain Kit (Thermo Fisher). Gating strategies for PBMCs analyzes were as previously described[15] and can be found in Figures S2 and S3.

Histology and immunofluorescence staining

All specimens were sectioned into 5 μm sections from formalin-fixed, paraffin-embedded tissue. Sections were dewaxed in xylene and rehydrated using serial ethanol baths in decreasing concentrations. Specimens were histopathologically evaluated with conventional hematoxylin and eosin (H&E) staining. Further evaluation was performed via immunofluorescence staining. Antigen retrieval was performed with citrate buffer pH 6 (Agilent Dako) in a pressure cooker (BioCare Medical) programmed at 110°C for 15 min. Sections were incubated with primary antibodies rabbit-anti-human CD4 (Novus Biologicals) at 1:200 and mouse-anti-human CD8 (Abcam) at 1:50 overnight at 4°C. Afterward, biotinylated secondary antibodies goat-anti-rabbit (Vector) and horse-anti-mouse (Vector) were both incubated at 1:200 for 1 h at room temperature followed by Streptavidin-AF546 conjugate (Invitrogen) and Streptavidin-AF647 conjugate (Invitrogen), respectively, for 30 min at room temperature. Sections were mounted with ProLong Gold Antifade Reagent with DAPI (Invitrogen) and coverslipped. Immunofluorescence-stained sections were photographed using a fluorescence microscope (EVOS FL Auto 2, Invitrogen) and processed with ImageJ software.

Immunohistochemistry

All specimens were sectioned into 5 μm sections from formalin-fixed, paraffin-embedded tissue. Immunohistochemical staining was performed using an automated Ventana BenchMark Stain System (Roche). Antibodies used were ready-to-use rabbit anti-human CD3 (Roche), rabbit polyclonal anti-CD31 (Abcam) at 1:50, rabbit anti-human CD45 (Cell Signaling) at 1:500 and rabbit anti-mouse CD45 (Cell Signaling) at 1:500. Stained sections were photographed using an Axio Imager M2 microscope (Zeiss) and processed with ImageJ and Photoshop software.

RNA extraction

We obtained six consecutive 10 μm sections from formalin-fixed paraffin-embedded (FFPE) skin punch biopsies taken at different time points. Deparaffinization with Xylene and RNA extraction were performed in sterile 1.5 mL microcentrifuge tubes with the RNeasy FFPE Kit (Qiagen), according to the manufacturer's instructions. The concentration and purity of the isolated total RNA were measured using a NanoDrop 2000 spectrophotometer (Thermo Fisher) at the Center for Advanced Molecular Diagnostics (CAMD) Research Core of the Brigham and Women's Hospital. The absorbance ratio at 260/280 was used to determine RNA quality.

NanoString nCounter assay for mRNA gene expression assay

To investigate intragraft gene expression changes during rejection episodes, 18 limb allograft biopsies taken between December 2013 and November 2018 were retrieved from the pathology archive at Brigham and Women's Hospital, Boston. We obtained a total of ten biopsies from rejection and eight from nonrejections episodes. From the 18 samples analyzed, one did not pass quality control (nonrejection) and was excluded from the analysis. For nonrejection episodes, these included five biopsies with Banff grades 0 and two samples with Banff grades 0/1. For rejection episodes, samples included two biopsies with Banff grades 2, two samples with Banff grade 2/3, and six biopsies with Banff grades 3. We then analyzed 770 genes with the NanoString nCounter PanCancer Immune Profiling Gene Expression (GX) Codeset. Gene expression was measured on 100–200 ng of extracted RNA. Samples were processed on the NanoString nCounter Analysis System (NanoString Technologies) following the manufacturer's instructions at the CAMD Research Core of the Brigham and Women's Hospital. Images were processed into RCC files from two batches of two different lots of reagents.

We normalized raw gene expression counts, batch effect, background correction, data quality control and analyzed the data with the nSolver Analysis Software (Version 4.0.70). Twenty-seven reference genes (*EIF2B4*, *PRPF38A*, *DDX50*, *MRPS5*, *AMMECR1L*, *CNOT4*, *COG7*, *TLK2*, *ZNF143*, *DHX16*, *SAP130*, *TBP*, *SDHA*, *NOL7*, *ZC3H14*, *TMUB2*, *EDC*, *FCF1*, *PPIA*, *AGK*, *HDAC3*, *POLR2A*, *SF3A3*, *USP39*, *ZNF346*, *GUSB* and *MTMR14*) were used for normalization. We used the quality control parameters recommended by the manufacturer.

QUANTIFICATION AND STATISTICAL ANALYSIS

For flow cytometry data, we used paired t-test for paired two group comparations. In animal experiments, we used unpaired Student's t-test for comparison of the two independent groups. All statistical tests were two-sided with a type 1 error rate of 0.05 to determine statistical significance. Prism software was used for data analysis and drawing graphs (GraphPad Software, Inc., San-Diego, CA).

For the NanoString analyzes, differentially expressed genes (DEGs) between rejection and nonrejections samples were analyzed using the nSolver Analysis Software (Version 4.0.70). Samples were not paired in this analysis. Because of the low number of samples, a gene was considered differently expressed when the comparison between groups reached a log2 fold change > 2 and an unadjusted p-value < 0.01. The $\log_2$ fold change of genes assessed was transformed into Z-scores and a heatmap was created using Morpheus matrix visualization and analysis tool from the Broad Institute (https://software.broadinstitute.org/morpheus). Unsupervised principal component analysis of the top 57 DEGs clustering the samples with rejection compared to nonrejection events as generated using the web tool ClustVis[43] using their default configurations. Gene Ontology terms were identified using the PANTHER tool (Protein Analysis Through Evolutionary Relationships, http://pantherdb.org).[44] All the 57 DEGs were used as an input with *Homo sapiens* as the organism and enriched for GO (biological processes) terms only. Fisher's one-tailed test with Benjamini-Hochberg False Discovery Rate (FDR p value) for multiple testing corrections was used as statistics. A Volcano plot showing differentially expressed genes (DEGs) in rejection in relation to nonrejection was generated using nSolver Analysis Software (Version 4.0.70). Log2 fold change is represented in the X axis, and the Y axis displays −log10 of each gene's p value.

ADDITIONAL RESOURCES

The study was registered at ClinicalTrials.gov (NCT01293214).

Cell Reports Medicine, Volume *3*

Supplemental information

T cell-attracting CCL18 chemokine is a dominant rejection signal during limb transplantation

Thiago J. Borges, Phammela Abarzua, Rodrigo B. Gassen, Branislav Kollar, Mauricio Lima-Filho, Bruno T. Aoyama, Diana Gluhova, Rachael A. Clark, Sabina A. Islam, Bohdan Pomahac, George F. Murphy, Christine G. Lian, Simon G. Talbot, and Leonardo V. Riella

Supplemental Information

Borges et al.

T cell-attracting CCL18 chemokine is a dominant rejection signal during limb transplantation

Supplementary Figures:

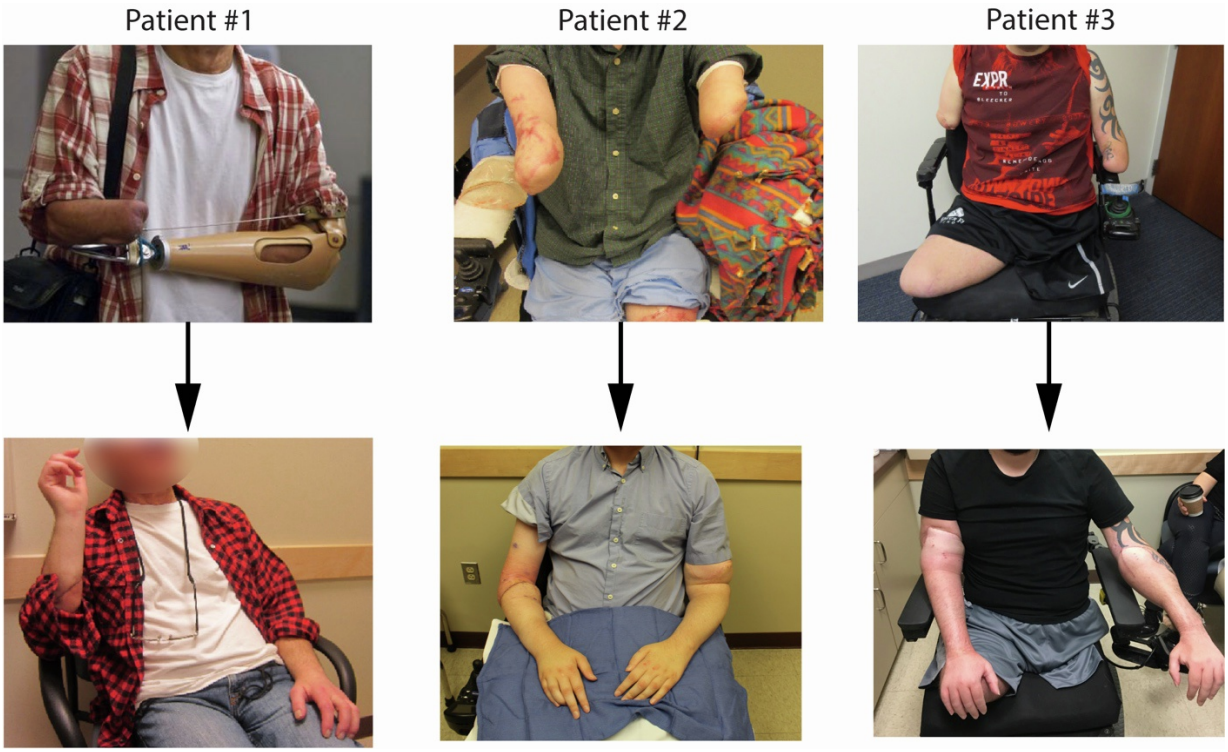

Figure S1. Photographs of the three patients before and after the transplantation. Patients provided written consent for the publication of their pictures. Related to Figure 1.

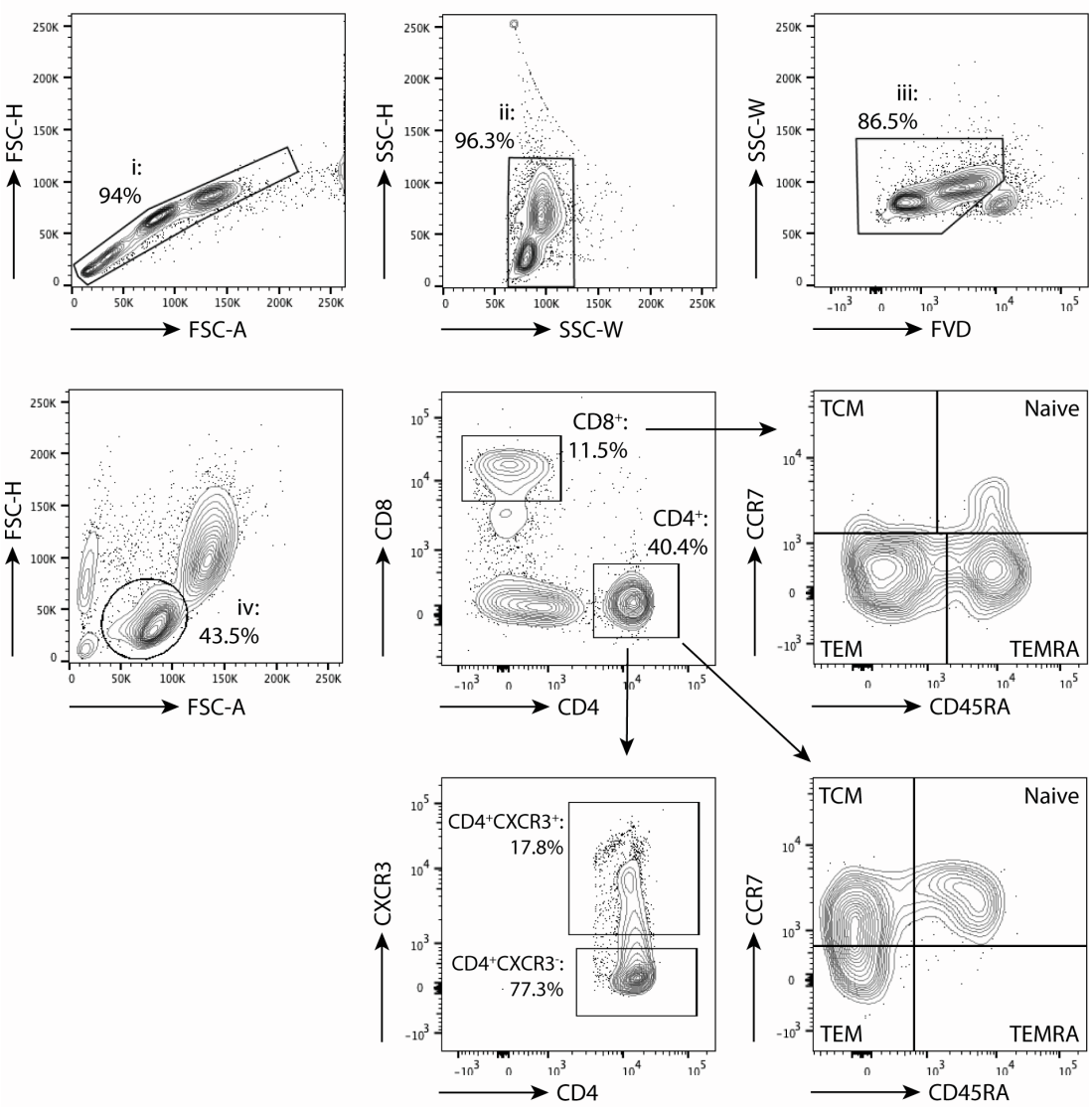

Figure S2. Gating strategy of the T-cell populations from peripheral blood analyzed in this study. All samples were analyzed with FlowJo software. FVD = Fixable viability dye. Related to Figure 1.

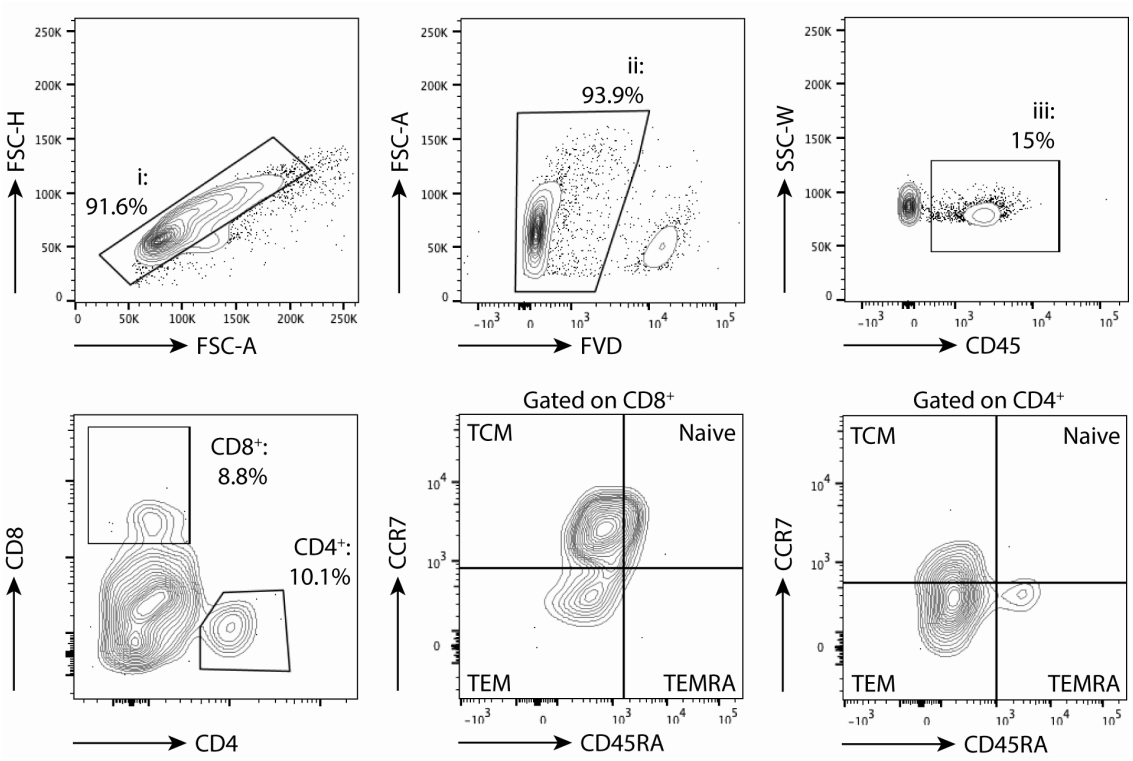

Figure S3. Gating strategy of the T-cell populations from allograft and native skin of upper extremities recipients. All samples were analyzed with FlowJo software. FVD = Fixable viability dye. Related to Figure 2.

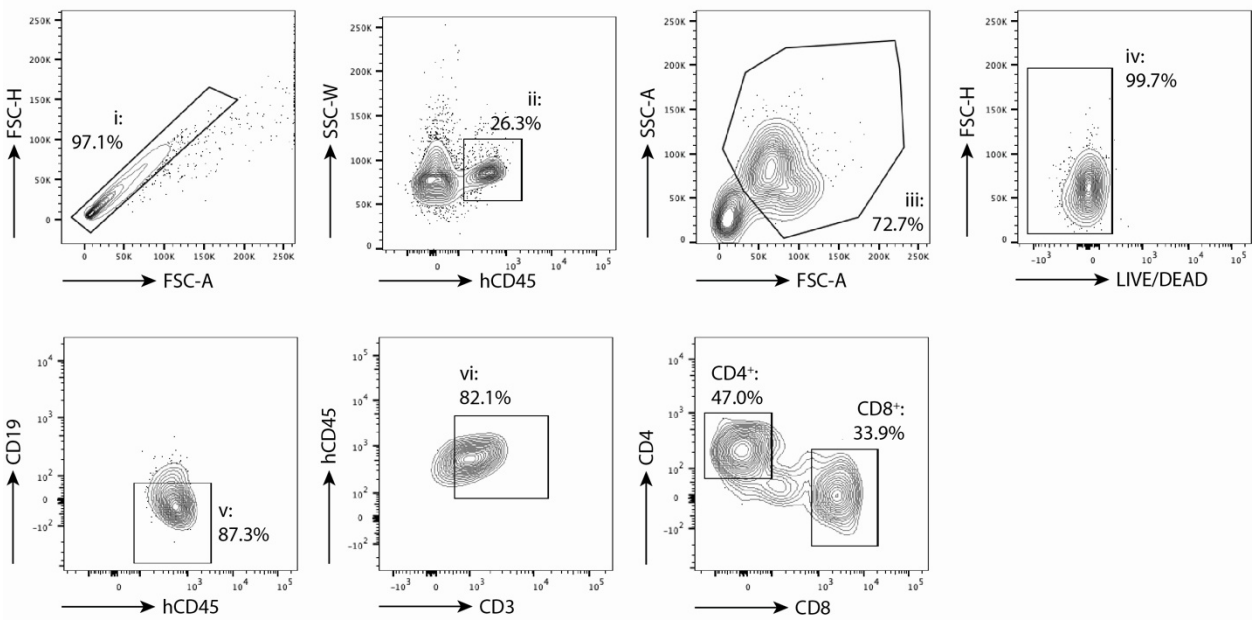

Figure S4. Gating strategy of the T-cell populations from xenografts transplanted onto NSG recipient mice. All samples were analyzed with FlowJo software. Related to Figure 6.